Journal of Applied Physics ARTICLE pubs.aip.org/aip/jap

Doping dependence of boron–hydrogen dynamics in crystalline silicon

Cite as: J. Appl. Phys. **136**, 085703 (2024); doi: 10.1063/5.0215089
Submitted: 22 April 2024 · Accepted: 11 August 2024 ·
Published Online: 28 August 2024

P. Vieira Rodrigues,[1] B. Hammann,[1,2,a)] N. Aßmann,[3] J. Schön,[1,2] W. Kwapil,[1,2] T. Niewelt,[1,2,4] F. Schindler,[1] E. V. Monakhov,[3] and M. C. Schubert[1]

AFFILIATIONS

[1]Fraunhofer Institute for Solar Energy ISE, Heidenhofstraße 2, 79110 Freiburg, Germany
[2]Department of Sustainable Systems Engineering (INATECH), University of Freiburg, Emmy-Noether-Str. 2, 79110 Freiburg, Germany
[3]Centre for Materials Science and Nanotechnology, University of Oslo, 0315 Oslo, Norway
[4]School of Engineering, University of Warwick, Coventry CV47AL, United Kingdom

[a)]**Author to whom correspondence should be addressed:** benjamin.hammann@ise.fraunhofer.de.

ABSTRACT

In this contribution, we investigate the formation and dissociation of boron–hydrogen (BH) pairs in crystalline silicon under thermal equilibrium conditions. Our samples span doping concentrations of nearly two orders of magnitude and are passivated with a layer stack consisting of thin aluminum oxide and hydrogen-rich silicon nitride (Al_2O_3/SiN_x:H). This layer stack acts as a hydrogen source during a following rapid thermal annealing. We characterize the samples using low-temperature Fourier-transform infrared spectroscopy and four-point-probe resistivity measurements. Our findings show that the proportion of hydrogen atoms initially bound to boron (BH pairs) rises with increasing boron concentration. Upon isothermal dark annealing at (163 ± 2) °C, hydrogen present in molecular form, H_2, dissociates at a rate directly proportional to the concentration of boron atoms, $\propto [B^-]$, leading to the formation of BH pairs. With prolonged annealing, an unknown hydrogen complex is formed at a rate that is inversely proportional to the square of the boron concentration, $\propto 1/[B^-]^2$, resulting in the disappearance of BH pairs. Based on experimental observations, we derive a kinetic model in which we describe the formation of the unknown complex through neutral hydrogen H^0 binding to a sink. Additionally, we investigate the temperature dependence of the reaction rates and find that the H_2 dissociation process has an activation energy of (1.11 ± 0.05) eV, which is in close agreement with theoretical predictions.

I. INTRODUCTION

Hydrogenation processes are crucial for semiconductors and have been widely applied for decades to different technologies.[1–7] These processes are aimed at, e.g., influencing the electronic properties of a material, given the ability of hydrogen to bind to impurities and structural defects, resulting in an electrical passivation. Silicon solar cells, in particular, benefit from the decrease in charge carrier recombination rate due to hydrogen passivation. A typical hydrogenation procedure for solar cells involves depositing a hydrogen-rich dielectric layer of silicon nitride (SiN_x:H) on top of the wafer.[8–10] The deposited silicon nitride acts as a capping layer and is optimized to decrease the reflectivity of the material.[11] Hydrogen is then introduced from the SiN_x:H layer into the silicon bulk during a high-temperature "fast-firing" step.[8,9,12,13]

On the other hand, it has been demonstrated that hydrogen is involved in the activation of light- and elevated-temperature-induced degradation (LeTID)[14–20] and might also play an essential role in surface-related degradation (SRD) events.[18,19,21–25] Contrary to the main goal of performance improvement, these degradation phenomena cause unwanted efficiency losses that occur over long time scales and under typical operating conditions.[26] Given the

ample use of hydrogen-containing functional layers in commercially available solar cell technologies, it is imperative to better understand the behavior of hydrogen. In this context, investigating the link between hydrogen, LeTID, and SRD is key, as it will clarify the underlying degradation mechanisms and help to improve mitigation strategies.

Direct quantification of hydrogen in silicon is demanding, since the investigated concentrations are typically below the detection limits of conventional methods. However, hydrogen can be indirectly monitored through the dynamics of the boron–hydrogen (BH) complex. Such an indirect approach has been used, for instance, by Walter *et al.*,[27] Winter and Herguth,[24] and by us in previous publications.[18,19,25] It was observed that BH pairs, LeTID, and SRD defects not only evolve in parallel but are also connected through the same overall reaction. This fact highlights the importance of BH-dynamics as a fundamental tool to investigate hydrogen-induced degradation mechanisms.

A detailed analysis of BH-dynamics in c-Si has been conducted, e.g., by Voronkov and Falster.[28] They revisited available literature and formulated a kinetic model to describe the literature data.[29–31] This kinetic model, with parameters recently updated,[32] contains hydrogen reactions that imply a strong doping dependence of both formation and dissociation of BH pairs. This doping dependence has not been extensively tested, although it is originally based on samples with just two different boron concentrations ($N_B \approx 10^{16}$ and $10^{17}\,cm^{-3}$).[29,31] In addition, these samples were exposed to a H_2 atmosphere at temperatures close to 1300 °C. Such a hydrogenation method differs significantly from the standard processing sequences employed in today's photovoltaic industry, as outlined above.

To further investigate the doping dependence of BH-dynamics in c-Si, we present herein experimental data with doping concentrations spanning one and a half orders of magnitude ($N_B \approx 1.6 \times 10^{15}$ to $7 \times 10^{16}\,cm^{-3}$). Moreover, we use samples subjected to a hydrogenation process that is relevant to and representative of modern solar cell manufacturing. We observe that the kinetics of BH pairs strongly depends on the doping concentration. In addition, we find that our experimentally observed trends are not in line with the dissociation mechanism suggested by Voronkov and Falster,[28] even when considering their re-evaluated parameters.[32]

In this work, we combine data from our earlier studies[18,19] with a new experimental study to systematically analyze the kinetics of BH pairs. We start the analysis from scratch, using an *abstract three-state model*. Based on this kinetic analysis, we deduce elementary reactions that give rise to the experimentally observed doping dependencies. In addition, we develop a detailed kinetic model that not only is capable of describing our experimental data well, particularly the doping dependence but can also be applied to data obtained by other authors. Furthermore, we investigate the temperature dependence of the three-state and detailed kinetic models using data from both Winter *et al.*[33] and Acker *et al.*[34] Last, we discuss a potential mechanism behind the dissociation of BH pairs.

II. THEORETICAL BACKGROUND

Early work from McQuaid *et al.*[30,35,36] and Binns *et al.*[29] utilized infrared (IR) absorption spectroscopy to investigate the solubility of hydrogen in crystalline silicon. Their experiments were conducted on B-doped, ∼2 mm thick samples hydrogenated via a high-temperature H_2-plasma technique and subsequently quenched to room temperature. They found BH pairs present after quenching, with the BH concentration increasing upon annealing at 175 °C. These results implied the existence of a hydrogen reservoir, which, however, could not be detected with their technique.

Later, Pritchard *et al.*[31] identified, thanks to long-path-length samples of ∼17 mm thickness, that the "hidden" hydrogen reservoir exists in the form of weakly IR-active H_2 molecules. The annealing of these samples led to a gradual decrease in $[H_2]$, with simultaneous rise in [BH]. The sum of hydrogen concentration in both states $2 \times [H_2] + [BH]$, estimated from the integrated IR absorption coefficients, remained constant during annealing and close to the total hydrogen concentration measured with SIMS. It was concluded that essentially all of the hydrogen atoms released from the H_2 reservoir bind to boron, i.e., there is a conversion from hydrogen molecules to boron–hydrogen pairs. Notably, Pritchard *et al.*[31] found that the initial loss rate of hydrogen molecules was proportional to the concentration of electrically active boron atoms, i.e., $\propto [B^-]$.

The investigations from Binns *et al.*[29] and Pritchard *et al.*[31] also demonstrated that the BH complex disappears after prolonged isothermal annealing. Data on BH dissociation are explicitly shown by Binns *et al.*,[29] but only mentioned by Pritchard *et al.*[31] as a brief statement. During the dissociation of BH pairs, no evidence of H_2 re-formation was ascertained. Moreover, effusion experiments in combination with SIMS profiling imply that hydrogen stays inside the crystalline silicon after BH dissociation at the temperatures studied herein.[37,38] If hydrogen out-diffusion is not significant during BH dissociation, the disappearance of BH pairs implies that the released hydrogen binds to a partner and forms another complex, which remains to be identified.

For the unidentified complex, Voronkov and Falster[28] suggest that the binding partner of hydrogen is hydrogen itself, resulting in a molecular configuration different from H_2 called H_{2C}. According to their suggested mechanism, H_{2C} might correspond to the dimer H_2^*, which is IR-active and consists of two hydrogen atoms located at opposite sites of a Si atom. However, the local vibration mode (LVM) assigned to H_2^* defects was not detected during the loss of BH pairs.[31] This fact correlates with other reports that found H_2^* solely in irradiated silicon.[29] In addition, first-principles calculations suggest that a hydrogen molecule other than H_2 (and the dimeric H_2^* structure) is unlikely to occur in silicon.[39] Experimentally, Pritchard *et al.*[31] observed the appearance of a LVM associated with the vacancy-hydrogen VH_4 complex upon the dissociation of BH pairs. Therefore, it is possible that hydrogen coming from BH pairs might be involved in a reaction leading to VH_4. This possibility, however, needs further investigation and we address some open questions below.

A. Kinetic models for the formation and dissociation of BH pairs

As mentioned before, Voronkov and Falster[28] proposed a model for the kinetics of BH pairs in crystalline

silicon, which incorporates the following elementary reactions:

$$H_2 + h^+ \rightleftharpoons H^+ + H^0, \tag{1a}$$

$$BH + H^+ \rightleftharpoons H_{2C} + B^- + 2h^+, \tag{1b}$$

where H^+ and H^0 are positively charged and neutral hydrogen atoms, respectively, and h^+ is a hole.

Equation (1a) represents the dissociation of hydrogen molecules into atomic form. This process was suggested to occur when H_2 captures a hole.[28] Atomic hydrogen in p-type silicon is mostly present in a positive charge state,[40] which can bind to a negatively charged boron atom, resulting in a BH pair. Voronkov and Falster[28] argue that the trapping/releasing of H^+ by boron occurs fast compared to the annealing timescales. Therefore, H^+ and BH pairs are approximately in equilibrium with the equilibrium constant

$$K_{BH} = \frac{[BH]}{[H^+][B^-]}. \tag{2}$$

The disappearance of BH pairs upon long-term annealing is tentatively ascribed to the formation of a hypothetical hydrogen molecule termed H_{2C},[28] resulting in the reactivation of boron atoms [compare Eq. (1b)].

Equation (1a) was formulated on the grounds that the initial loss rate of hydrogen molecules scales with the boron concentration (compare Pritchard *et al.*[31]). On the other hand, Eq. (1b) was assumed to best reproduce the shape of a hydrogen profile in a p–n junction structure.[28] As already mentioned above, the existence of the alleged H_{2C} molecule is still unclear, since there are neither experimental findings nor conclusive *ab initio* calculations supporting this hypothesis. To account for such an uncertainty in our kinetic analysis, the unknown complex formed with the hydrogen dissociated from BH pairs is termed $\mathcal{X}$ throughout this contribution.

Following the equilibrium-argument between H^+ and BH, the model from Voronkov and Falster [cf. Eq. (1), also termed the *VF model*] can be regarded as the interaction between three states, H_2, BH, and $\mathcal{X}$, with two subsystems $H_2 \leftrightarrow$ BH and BH $\leftrightarrow \mathcal{X}$. In our kinetic analysis, we abstract the VF model further to a so-called *abstract three-state model*, which consists of states *A*, *B*, and *C* representing H_2, BH, and the unknown $\mathcal{X}$, respectively (as similarly done in Refs. 33, 34, and 41).

Based on an analysis with the abstract three-state-model, we develop a detailed model that contains the various hydrogen complexes and the different charge states of atomic hydrogen. We refer to this model as a *detailed kinetic model* throughout this contribution. Both the abstract and detailed models are more thoroughly discussed in their respective sections [cf. Eqs. (6) and (7) in Sec. V, and Eqs. (13) and (14) in Sec. VI].

III. METHODOLOGY

A. Sample preparation

Our samples consist of float-zone (FZ) Si wafers with doping concentrations ranging between 1.6×10^{15} and $7 \times 10^{16}\,\mathrm{cm}^{-3}$, processed according to the diagram depicted in Fig. 1. They have a thickness of 250 μm and are boron-doped with five different base doping concentrations. The samples are initially cleaned via a Radio Corporation of America (RCA) cleaning sequence and afterward undergo an oxidation step in a tube furnace at 1050 °C. This step dissolves typical FZ-Si defects[42] and potentially allows the out-diffusion of residual hydrogen that was found to be present in out-of-the-box FZ-Si wafers.[33] The grown SiO_x film is subsequently etched away, after which a $POCl_3$-diffusion takes place at 810 °C for one hour to getter the remaining impurities. The resulting phosphorus silicate glass (PSG) and highly P-doped layers are then removed, approximately 5 μm on each side, followed by another RCA cleaning. A thin aluminum oxide (Al_2O_3) film of 5 nm is deposited on both sides of the wafer via atomic layer deposition (ALD) to ensure a better surface passivation quality. The samples are further covered with 150 nm-thick layers of hydrogen-rich silicon nitride (SiN_x:H) on top of the Al_2O_3 films on both sides via PECVD. Subsequently, the wafers undergo rapid thermal annealing (RTA) with a measured peak temperature T_{peak} of 800 °C and a cooling rate of ca. 60 K s^{-1} above 550 °C. During this high-temperature step, hydrogen diffuses from the SiN_x:H layers into the silicon bulk.[12] After RTA, samples of the same doping concentration are divided into two sets of sister wafers.

In the first set, the passivation stack Al_2O_3/SiN_x:H is entirely removed from both sides of the wafer by immersion in a 10% hydrofluoric acid solution for approx. 15 min. After that, the bare silicon wafer is cleaved into 10 × 10 mm^2 pieces with a laser-based process.

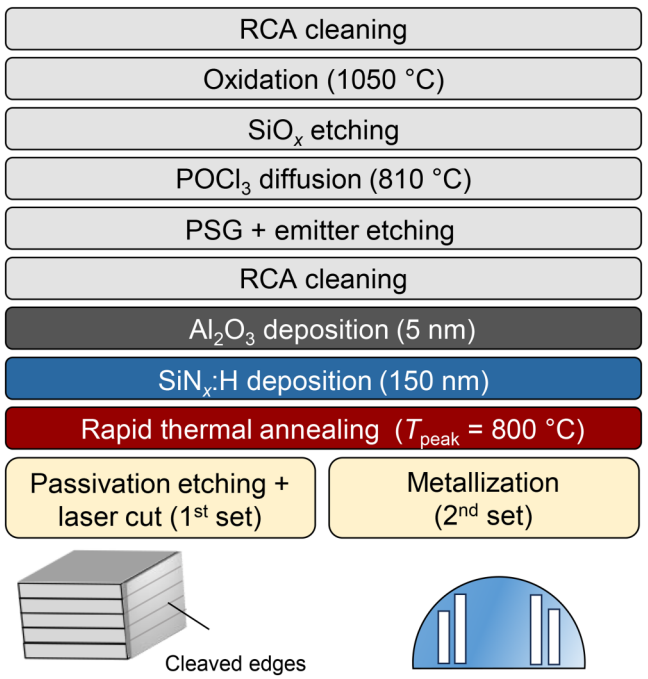

FIG. 1. Process diagram showing the sequential manufacturing steps, from top to bottom, applied to the samples investigated in the present work. A schematic sample layout is shown at the bottom of the diagram.

In the second sample set, the passivation stack Al_2O_3/SiN_x:H is locally removed on one side of the wafer. Thin aluminum foils are then joined to the exposed silicon substrate in the ablated areas (for more process details, compare Ref. 43). It is important to note that this metallization process does not involve high-temperature steps that could influence the configuration of hydrogen.

B. Design of the experiment

Optical measurement of small hydrogen concentrations benefits from long optical path lengths. Since the investigated wafers are so thin, we chose to investigate stacks made from the laser cleaved tokens (compare Ref. 44). This format ensures a sufficiently long path length needed for detecting H_2 molecules. In addition, the cleaved edges of the pieces help to minimize reflection losses. The piece stack is characterized with low-temperature Fourier-transform infrared spectroscopy (FT-IR) to measure the initial concentrations of boron–hydrogen pairs $[BH]_{ini}$ and hydrogen molecules $[H_2]_{ini}$.[31,44]

The metallized wafers from the second sample set are annealed on a light-tight hotplate at (163 ± 2) °C. Throughout annealing, the samples are removed at regular intervals and characterized *ex situ* with a four-point-probe (4PP) setup at 25 °C to measure the bulk resistivity. The resistivity measurements serve to track changes in the equilibrium hole density Δp_0 caused by the interaction between hydrogen and boron. For instance, to form BH pairs, neutral hydrogen molecules must first dissociate. The resulting positively charged atomic hydrogen atoms H^+ contribute electrons to the lattice, resulting in a decrease of p_0. During this process, H^+ and B^- form electrically neutral BH pairs.[45,46] Conversely, the electrical activity of boron atoms is restored upon the dissociation of H^+ and the formation of the presumably electrically neutral complex $\mathcal{X}$, resulting in an increase of p_0. The evolution of BH pairs during annealing can be approximated by combining the results from FT-IR and 4PP,

$$[BH] \approx [BH]_{ini} - \Delta p_0. \tag{3}$$

Note that Eq. (3) is only an approximation, as it is not possible to discern between $(H^+ + B^-)$ and BH solely on the basis of resistivity measurements. Given that $[H^+]$ becomes increasingly significant for lower doping concentrations (cf. Ref. 28), our simulations are always performed with $[BH] + [H^+]$.

1. Further sample sets

Apart from the sample sets described in Sec. III A, we have also fabricated a *reference sample set*, consisting of wafers subjected only to RCA cleaning, oxidation, and metallization (first, second, and last steps in Fig. 1). We characterized our reference samples with 4PP under annealing at (163 ± 2) °C and found no resistivity changes over 3000 h except slight variations in the lowest doped sample (compare Appendix B). This demonstrates that the employed oxidation step is able to remove the residual hydrogen that can be found in out-of-the-box FZ-Si wafers.[33] Therefore, we assume that all hydrogen measured in our experiments is diffused from the SiN_x:H layer into the bulk during the RTA step.

To complement the analysis of the present work, we include additional experimental data from our previous publications[18,19] and from other authors.[33,34] These complementary data are all based on samples with $N_B \approx 1.5 \times 10^{16}$ cm^{-3} and very similar processing and characterization methods compared to those employed herein. Our data published in Hammann *et al.*[18,19] are annealed at (175 ± 2) °C and feature a variation in hydrogen concentration, instead of boron. Such a variation is induced by dissimilar wafer thicknesses and temperature profiles during RTA. The data from Winter *et al.*[33] and Acker *et al.*[34] cover a broad range of annealing temperatures from 160 up to 290 °C. Since these data do not contain information about $[BH]_{ini}$ or $[H_2]_{ini}$, we estimate both quantities using the approach described in Appendix A. To distinguish between the different complementary data sets, we term them *boron variation* (this work), *hydrogen variation* (Hammann *et al.*[18,19]), and *temperature variation* (Winter *et al.*[33] and Acker *et al.*[34]).

C. Sample characterization

1. Cryogenic FT-IR spectroscopy

The FT-IR spectroscopy measurements are performed with a Bruker IFS 125HR spectrometer at 5 K, equipped with a globar source and a KBr beam splitter in the mid-infrared range. The calibration coefficients $A_{BH} = (3.0 \pm 0.3) \times 10^{15}$ cm^{-1} (Ref. 35) and $A_{H_2} = (8.0 \pm 0.1) \times 10^{17}$ cm^{-1} (Ref. 47) are used to calculate the concentration of BH pairs and H_2 molecules with vibration lines at 1904 cm^{-1} and 3618.4 cm^{-1}, respectively. More details about the measurement of hydrogen-related defects using infrared spectroscopy can be found in the study by Weiser *et al.*[44]

2. Four-point-probe measurements

The wafer bulk resistivity ρ_{bulk} can be measured, e.g., with an eddy-current sensor as proposed by Walter *et al.*,[27] resulting in a relative uncertainty of $\sim 2\% \times \rho_{bulk}$. Alternatively, improved accuracy can be achieved by directly contacting the silicon substrate in a four-terminal configuration (4PP). When combining 4PP measurements with precise temperature control, the relative uncertainty is greatly improved (compare Ref. 24). We have assessed our uncertainty to $\sim 0.1\% \times \rho_{bulk}$.

The sample layout used in this work for bulk resistivity measurements is illustrated in Fig. 1 (bottom right) and follows the design proposed by Winter and Herguth.[24] The bulk resistance R is measured with a 2002 series Keithley sourcemeter. For thin films with uniform thickness, the bulk resistivity can be calculated as

$$\rho_{bulk} = R \frac{W}{f_g}, \tag{4}$$

where W is the sample thickness and f_g is a factor that accounts for the geometric properties of the experimental setup, e.g., sample dimensions and positioning of the probes. The geometric factor of our sample layout is determined via numerical simulation with *Quokka3*®.[48,49]

Sample resistivity is a function of charge carrier mobilities that are strongly temperature dependent. Therefore, stable and reproducible temperatures must be ensured during the measurements. For this reason, thin metallic needles press the sample against a chuck made of copper, helping to achieve good thermal contact. The temperature of the chuck is regulated to 25 °C with Peltier

elements and controlled by a resistance thermometer. The calculated ρ_{bulk} is converted into hole concentration using the mobility model from Klaassen *et al.*[50,51] The changes in hole concentration are calculated according to Eq. (5),

$$-\Delta p_0 = -(p_0(t) - p_0(t_0)), \tag{5}$$

where $p_0(t_0)$ and $p_0(t)$ are the equilibrium hole densities in a reference state at time t_0 and in a subsequent state at time t, respectively. Note the use of the minus sign here, since a decrease in Δp is interpreted as an increase in [BH] [compare Eq. (3)]. Furthermore, throughout this work, samples are sometimes labeled with their respective doping concentration. We use the notation N_B to refer to the total boron concentration, which is constant over time, and the notation $[B^-]$ to refer to the active boron concentration.

IV. EXPERIMENTAL RESULTS

A. BH pairs after rapid thermal annealing

Figure 2 shows the initial concentrations of boron–hydrogen pairs $[BH]_{ini}$ and hydrogen in molecular form $2[H_2]_{ini}$ measured by cryogenic FT-IR spectroscopy after rapid thermal annealing, for differently doped samples. Percentage values indicate the concentration ratio between BH pairs and total hydrogen, calculated as $[H]_{tot} = 2 \times [H_2]_{ini} + [BH]_{ini}$.

As it can be seen in Fig. 2, there is an allocation of hydrogen complexes after RTA. The total hydrogen concentration ranges between 1.6×10^{15} and 2.8×10^{15} cm^{-3}, while the initial concentration of BH pairs increases with doping by orders of magnitude (see inset of Fig. 2). On the one hand, $[BH]_{ini}$ represents only a small fraction of the total boron content, up to $\sim 2\% \times N_B$. On the other hand, $[BH]_{ini}$ can constitute a significant share of the total hydrogen present, reaching >70 % for our highest investigated doping concentration.

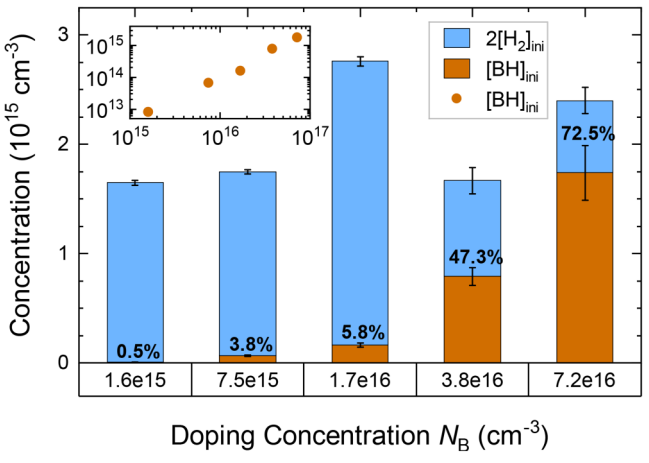

FIG. 2. Initial concentrations of boron–hydrogen pairs $[BH]_{ini}$ and hydrogen in molecular form $2[H_2]_{ini}$ measured by cryogenic FT-IR spectroscopy after RTA, for differently doped samples. The percentage values describe the share of $[BH]_{ini}$ with respect to the total hydrogen concentration. Additionally, the $[BH]_{ini}$ data are plotted on a logarithmic scale in the inset.

B. BH pairs during isothermal dark annealing

Figure 3 shows the evolution of the hole concentration during isothermal dark annealing at (163 ± 2) °C for different boron concentrations, offset by the respective initial BH pair concentration. A decrease in hole concentration (i.e., an increase in $-\Delta p_0$) is observed for initial annealing times in Fig. 3. This can be attributed to the dissociation of H_2 into atomic hydrogen, which charges positively by emitting electrons that recombine with free holes, effectively reducing the hole concentration. Then, H^+ pairs with B^-, which does not lead to further hole concentration changes. The BH pair formation continues until a maximum concentration $([BH]_{ini} - \Delta p_0)_{max}$ is reached. In sequence, an increase in hole concentration (i.e., a decrease in $-\Delta p_0$) is observed. This can be attributed to the splitting of BH, which results in the release of hydrogen atoms that we believe to recharge in the formation of an unknown hydrogen complex ($\mathcal{X}$).

Two features are prominent in the boron–hydrogen dynamics of differently doped samples. First, the maximum amount of BH pairs reached during the anneal increases with higher boron concentration, i.e., the attained $([BH]_{ini} - \Delta p_0)_{max}$ values increase with doping. Second, the rates of formation and dissociation of BH pairs seem to behave contrarily, in that the former increases with N_B, whereas the latter decreases with N_B.

C. Comparison to the literature model

We first simulate the model from Voronkov and Falster with their recently updated parameters[32] and compare the results to our data, as shown in Fig. 4. The only input parameters are $[BH]_{ini}$ and $[H_2]_{ini}$ measured with FT-IR, temperature, and doping concentrations. It can be seen that the simulated evolution of $[BH] + [H^+]$ (dashed, light blue lines) and the experimental data (black symbols) show the same general trend of formation followed by dissociation of BH pairs.

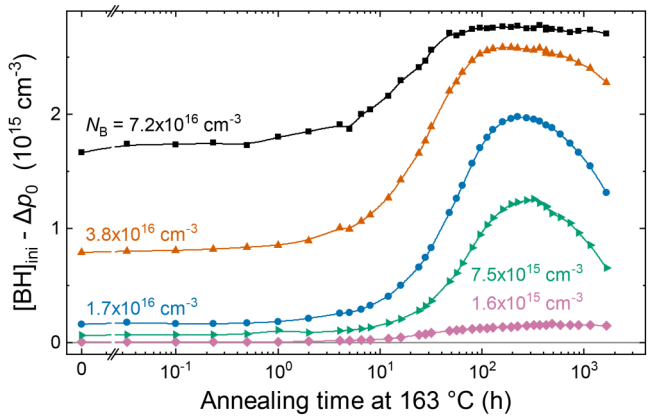

FIG. 3. Evolution of $-\Delta p_0$ during isothermal dark annealing at (163 ± 2) °C for different doping concentrations. The data are offset by the respective FT-IR measured initial BH pair concentration, $[BH]_{ini}$. Lines are guides to the eye (B-splines). Error bars are omitted for the sake of clarity.

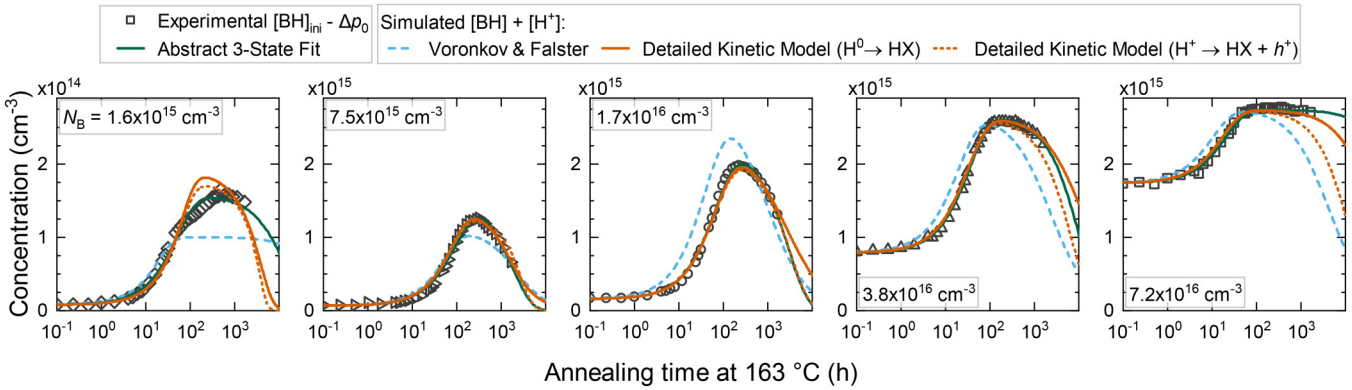

FIG. 4. Experimental $[BH]_{ini} - \Delta p_0$ data for samples with different boron concentrations annealed at 163 °C (black symbols), along with a fit using the *abstract three-state model* (dark green lines). Also shown are the simulations of $[BH] + [H^+]$ using the kinetic model from Voronkov and Falster[28] with updated parameters[32] (dashed, light blue) and the *detailed kinetic model* developed in this work (red). In the latter, the formation of $\mathcal{X}$ (=HX) is calculated for two different reactions: $H^0 + X \longrightarrow HX$ (solid lines) and $H^+ + X \longrightarrow HX + h^+$ (dotted lines). Note that the *detailed kinetic model* is discussed further below in Sec. VI.

During the formation of BH pairs, the simulated lines increase roughly at the same rate as the experimental data, for all doping concentrations. Therefore, the doping dependence of H_2 dissociation is most likely well reproduced by the VF model. Nevertheless, the rate constant used to simulate the H_2 dissociation is most likely overestimated, as the calculated increase in BH pairs is slightly faster than observed in the higher doped samples.

During the dissociation of BH pairs, the simulated curves decrease at similar rates compared to the experimental data only for the samples with doping concentrations of $N_B \approx 1.7 \times 10^{16}$ and 7.5×10^{15} cm^{-3}. For higher doping concentrations, the model predicts a significantly faster decrease than experimentally observed, whereas in the lowest doped sample, the predicted decrease appears to be slower. This demonstrates a problem of Eq. (1b) with predicting the influence of the boron concentration and implies that the VF model is probably flawed. We also observe deviations between the VF model and experimental data in the *hydrogen variation* set, as depicted in Fig. 5 (dotted line).

Before continuing with the analysis, we briefly discuss the maximum value $([BH]_{ini} - \Delta p_0)_{max}$. In the two highest doped samples of the *boron variation* set, we find $-\Delta p_{0,max} > 2[H_2]_{ini}$, i.e., the maximum change in equilibrium hole density is higher than the initial amount of hydrogen in molecular form. This apparent contradiction might be due to a variability in $[H_2]_{ini}$ between the sister wafers, uncertainties associated with the FT-IR measurement setup, or another undetected source of hydrogen. Since the FT-IR measurement of these two samples were done months after the resistivity measurement, we do not want to rule out the possibility of an $H_2 \rightarrow BH$ transformation already during the dark storage of these samples. Independent of the cause, $([BH]_{ini} - \Delta p_0)_{max}$ will never be reached by a simulation using the $[H_2]_{ini}$ values determined with FT-IR. As finding the cause of such an inconsistency is beyond the scope of this work, we choose to adjust the value of $[H_2]_{ini}$ in the two highest doped samples for a better match between simulation and experiment. The adjusted values of $[H_2]_{ini}$ can be found in Appendix D. Note that an adjustment of $[H_2]_{ini}$ for the remaining three lower doped samples would be able to offset the differences in $([BH]_{ini} - \Delta p_0)_{max}$ as well, but cannot account for the wrong doping dependence of Eq. (1b).

V. ANALYSIS

Given the observed discrepancies between our experimental results and the model by Voronkov and Falster, we decided to

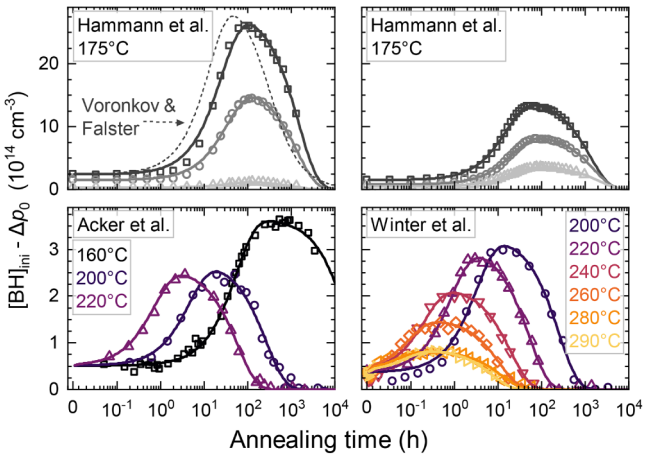

FIG. 5. Overview of the additional data sets evaluated in this study. *Hydrogen variation* set (Hammann *et al.*, top left: Ref. 18, top right: Ref. 19), and *temperature variation* set [Acker *et al.*[34] (bottom left) and Winter *et al.*[33] (bottom right)]. Note that the data of the sample with the lowest hydrogen concentration in the top left graph are not published in Ref. 18 despite being part of the sample set, but instead can be found in Ref. 53. Lines depict the evolution fitted with the *abstract three-state model*. In addition, the graph shows a simulation for one sample using the kinetic model by Voronkov and Falster[28] with the updated parameters[32] (dotted line).

reassess the situation at a fundamental level. To this end, we simplify the kinetics of BH pairs to an *abstract three-state model* consisting of first-order reactions given by Eq. (6),

$$A \rightleftharpoons B \rightleftharpoons C, \tag{6}$$

where A, B, and C represent H_2, BH, and $\mathcal{X}$, respectively. Note that we attribute these hydrogen complexes to their respective state in the mentioned order on the basis of the experimental, FT-IR based results from Pritchard *et al.*[31] and Binns *et al.*[29] (compare Sec. II). The *abstract three-state model* can, therefore, be described by the following set of ordinary differential equations:

$$\frac{\mathrm{d}[A]}{\mathrm{d}t} = -k_{\mathrm{AB}}[A] + k_{\mathrm{BA}}[B], \tag{7a}$$

$$\frac{\mathrm{d}[B]}{\mathrm{d}t} = k_{\mathrm{AB}}[A] - k_{\mathrm{BA}}[B] - k_{\mathrm{BC}}[B] + k_{\mathrm{CB}}[C], \tag{7b}$$

$$\frac{\mathrm{d}[C]}{\mathrm{d}t} = k_{\mathrm{BC}}[B] - k_{\mathrm{CB}}[C]. \tag{7c}$$

where k_{ij} denotes the rate constant of the corresponding reaction between states i and j.

Note that fitting k_{CB} to the data requires the final saturation level of BH pairs for very long annealing times to be known. However, given the experimental data of Fig. 4 measured in a timescale of approximately four months, we expect to observe such a potential saturation only after years of annealing. Furthermore, the data from the *temperature variation* set at 200 °C and above indicate that all BH pairs dissociate, meaning that the reverse reaction B ⟝ C, i.e., BH ⟝ $\mathcal{X}$, is not significant. Since no data on a potential saturation value exist for temperatures lower than 200 °C, we assume the same complete BH dissociation also at lower temperatures. Therefore, we further simplify the *three-state model* by setting $k_{\mathrm{CB}} = 0$, similar to Ref. 32.

Next, we fit the *three-state model* to the experimental data of the *boron*, *hydrogen*, and *temperature variations* sets such that the concentration of state $[B]$ matches the measured evolution of $[\mathrm{BH}]_{\mathrm{ini}} - \Delta p_0$. The following initial values are used: $[A]_{\mathrm{ini}} = 2[\mathrm{H_2}]_{\mathrm{ini}}$, $[B]_{\mathrm{ini}} = [\mathrm{BH}]_{\mathrm{ini}}$, and $[C]_{\mathrm{ini}} = 0$. The fitting is done in Python using the *lmfit* library[52] with the three fit parameters k_{AB}, k_{BA}, and k_{BC}. The fitted curves are depicted and compared to the experimental data in Fig. 4 (*boron variation*) and Fig. 5 (*hydrogen* and *temperature variation* sets). For those samples in which $-\Delta p_{0,\mathrm{max}} > 2[\mathrm{H_2}]_{\mathrm{ini}}$, we increase $[A]_{\mathrm{ini}}$ to the smallest value necessary for a coherent description (compare Appendix D).

A. Influence of participating reactants

In this subsection, we investigate the influence of $\mathrm{B^-}$, BH, and H_2 on the fitted rate constants. To this end, we use the fact that the *abstract three-state model* assumes first-order reactions. In that case, k_{AB}, k_{BA}, and k_{BC} must be regarded as effective rate constants, potentially leading to pseudo-first-order kinetics. Then, by plotting the effective rate constants against the concentration of different reactants in a double logarithmic plot, it is possible to assess the actual reaction order with respect to each reactant.

The reaction rate $-\mathrm{d}[A]/\mathrm{d}t = k_{\mathrm{AB}}[A]$ is largest around $[A]_{\mathrm{ini}}$, which equals the initial concentration of H_2. Therefore, we plot k_{AB} against $[\mathrm{H_2}]_{\mathrm{ini}}$ in Fig. 6(a) (orange symbols). In the graph, it can be seen that k_{AB} is constant for different concentrations of $[\mathrm{H_2}]_{\mathrm{ini}}$. As state A is a direct replication of hydrogen molecules, it follows that only one hydrogen molecule takes part in the H_2 dissociation reaction.

By investigating the relation between k_{AB} and the boron concentration in Fig. 6(c), a linear correlation can be observed. Since our resistivity-based method cannot distinguish between the acceptor $\mathrm{H^+}$ and a BH pair, i.e., we cannot observe the formation of BH pairs, these results give insights into the dissociation of hydrogen molecules. Therefore, we conclude that the dissociation of H_2 is a second-order reaction (being first order with respect to both $[\mathrm{H_2}]$ and $[\mathrm{B^-}]$),

$$-\frac{\mathrm{d}[\mathrm{H_2}]}{\mathrm{d}t} \propto [\mathrm{H_2}][\mathrm{B^-}]. \tag{8}$$

Equation (8) is in agreement with the results from Pritchard *et al.*[31] (compare Sec. II). Under the assumption that $[\mathrm{B^-}] \approx p$, it also agrees with the reaction proposed by Voronkov and Falster[28] [compare Eq. (1a)].

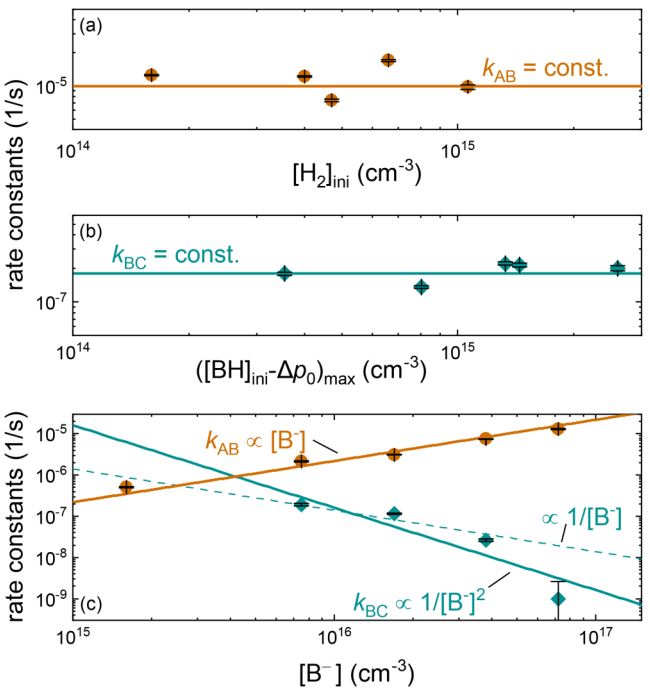

FIG. 6. Effective rate constants k_{AB} (orange) and k_{BC} (green) obtained by fitting the abstract three-state model [Eq. (7)] to the experimental BH-evolution of two different sample sets: *hydrogen variation* [(a) and (b)] and *boron variation* (c). In (a), k_{AB} is compared to the initial molecular hydrogen concentration, while in (b), k_{BC} is compared to the maximum $[\mathrm{BH}]_{\mathrm{ini}} - \Delta p_0$ value during dark annealing. In (c), both k_{AB} and k_{BC} are compared to the boron concentration.

The reaction rate $d[C]/dt = k_{BC}[B]$ is largest around the maximum value of $[B]$. Since state B is a direct replication of [BH], which can be approximated by $[BH]_{ini} - \Delta p_0$, we plot k_{BC} against the maximum value of $([BH]_{ini} - \Delta p_0)$, shown in Fig. 6(b) (green symbols).

Figure 6(b) shows that the k_{BC} values are constant for different concentrations of $([BH]_{ini} - \Delta p_0)_{max}$. This indicates that $B \rightarrow C$ is a first-order reaction with respect to $[B]$, which can be translated to being first order with respect to [BH].

The bottom graph of Fig. 6 investigates the relation between k_{BC} and boron concentration. It can be seen that the determined values of the rate constant k_{BC} decrease with boron concentration. A proportionality of $\propto 1/[B^-]^2$ (solid line) seems to fit all data points, whereas $\propto 1/[B^-]$ (dashed line) is also possible if one would exclude the highest doped sample. It is worth mentioning that the dissociation of BH pairs in the lowest doped sample appears to be influenced by more than just the BH kinetics (see Appendix B for more details). Furthermore, Fig. 4 shows that the evolution of BH pairs after long annealing times is not well reproduced by the *abstract three-state model* (dark green line), which is why k_{BC} of the lowest doped sample is excluded from Fig. 6.

We conclude that the formation rate of $\mathcal{X}$ is most likely given by

$$\frac{d[\mathcal{X}]}{dt} \propto \frac{[BH]}{[B^-]^2}. \tag{9}$$

Nevertheless, we leave room for doubt and in Sec. VI also investigate the dependence $\propto 1/[B^-]$, which would entail

$$\frac{d[\mathcal{X}]}{dt} \propto \frac{[BH]}{[B^-]}. \tag{10}$$

Finally, we want to briefly discuss the rate coefficient k_{BA}. We find that it decreases strongly with doping concentration, but does not follow a well-defined proportionality to $[B^-]$ (data not shown). As k_{BA} is sensitive to changes in $[A]_{ini}$, we attribute this undefined proportionality to uncertainties in the measured $[H_2]_{ini}$.

B. Temperature dependence

The temperature dependence of the rate constants obtained with the *abstract three-state model* is investigated next. To that end, we consider only similarly doped samples with $N_B \approx 1.5 \times 10^{16}$ cm^{-3} to distinguish between effects related to the boron concentration and those related to temperature. This includes all samples from the *temperature* and *hydrogen variation* sets and only one sample from the *boron variation* set.

Figure 7 shows k_{AB}, k_{BA}, and k_{BC} plotted against the reciprocal values of different temperatures. It can be seen that all rate constants present a typical Arrhenius behavior. Therefore, the data in Fig. 7 are fitted with an Arrhenius law following the equation

$$k_x = k_{x,0} \exp\left(\frac{-E_{A,x}}{k_B T}\right). \tag{11}$$

The resulting activation energies $E_{A,x}$ and pre-exponential factors $k_{x,0}$ are presented in Table I.

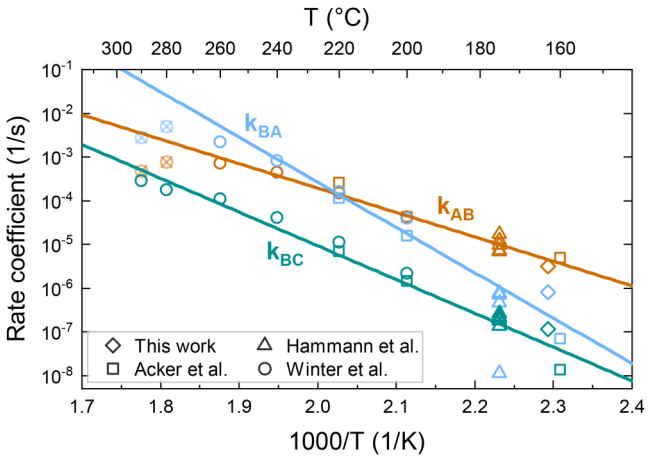

FIG. 7. Temperature dependence of rate constants determined from fitting the evolution of $[BH]_{ini} - \Delta p_0$ with the *abstract three-state model*, using data from the *hydrogen* (Hammann *et al.*[18,19]), *temperature* (Acker *et al.*[34] and Winter *et al.*[33]), and *boron variation* sets (this work). Note that only samples with $N_B \approx 1.5 \times 10^{16}$ cm^{-3} are considered. The lines are fits to an Arrhenius law, with some data points being excluded from the fit, which are depicted semi-transparent with a cross in the symbol. The fit results are presented in Table I.

We find the transition $A \rightarrow B$ ($H_2 \rightarrow$ BH) to have the lowest activation energy with (1.11 ± 0.05) eV. In comparison to other studies, we notice a small difference to the values determined by Winter *et al.* [(1.29 ± 0.07) eV][33] and Acker *et al.* [(1.20 ± 0.02) eV].[34] This difference can be explained by the simpler fit approach used by both authors, as their effective rate constant of the H_2 dissociation process is actually a superposition of k_{AB}, k_{BA}, and k_{BC}. Moreover, their fit approach assumes different values for $[A]_{ini}$, further impacting the results. On the other hand, a good agreement is found with the recent evaluation of Voronkov and Falster (1.15 eV)[32] on similar datasets. Importantly, the activation energy of k_{AB} determined here and by Voronkov and Falster[32] is very close to the boron-assisted H_2 dissociation barrier of 1.1 eV calculated by Coutinho *et al.*[54]

For the back reaction $A \leftarrow B$ ($H_2 \leftarrow$ BH), the highest activation energy of (2.05 ± 0.14) eV is found, while the BH dissociation reaction $B \rightarrow C$ (BH $\rightarrow \mathcal{X}$) shows an activation energy of (1.53 ± 0.07) eV. The latter diverges from the value of (1.22 ± 0.18) eV determined by Winter *et al.*,[33] but the discrepancy can again be attributed to the different assumed model as well as the inclusion of further data in the present work.

TABLE I. Pre-exponential factors k_0 and activation energies E_A of the rate constants k_{AB}, k_{BA}, and k_{BC} in Fig. 7, fitted with an Arrhenius law. Results are valid for doping concentrations $\approx 1.5 \times 10^{16}$ cm^{-3}.

	k_0 (s^{-1})	E_A (eV)
k_{AB}	$(2.8 \pm 3.7) \times 10^7$	1.11 ± 0.05
k_{BA}	$(1.4 \pm 4.4) \times 10^{17}$	2.05 ± 0.14
k_{BC}	$(2.6 \pm 4.4) \times 10^{10}$	1.53 ± 0.07

Note that the two data points of k_{AB} and k_{BA} fitted to the data from Winter *et al.*[33] at the highest temperatures (280 and 290 °C) deviate from the other data and are, therefore, excluded from the fit (depicted semi-transparent and with a cross in the symbol). The same behavior has also been observed by the authors themselves.[33] It is conceivable that, at such high temperatures, further hydrogen reactions begin to play a role, possibly even out-diffusion,[37,38] which could affect the kinetics and lead to the observed deviations.

VI. DETAILED KINETIC MODEL

The model derived above did not include much consideration of specific chemical reactions—hence the term *abstract three-state model*. In this section, we want to build upon the results and derive a *detailed kinetic model*. To that end, we first conceive possible elementary pairing paths including charge carriers for each hydrogen subsystem.

A. Subsystem $H_2 \nrightarrow BH$

Table II shows possible pathways for the $H_2 \rightarrow BH$ subsystem. We consider different hypotheses for the dissociation of hydrogen molecules, which could occur through thermal activation (No. 1), assistance of a boron atom (No. 2), assistance of one or more holes (Nos. 3 and 4), and assistance of both a boron atom and holes (Nos. 5 and 6). It can be seen that the kinetics of Reaction Nos. 2 and 3 give rise to Eq. (8). Both pairing paths yield a forward reaction rate directly proportional to the boron concentration, which is in accordance with our experimental results.

The mechanism associated with Reaction No. 3 was proposed by Voronkov and Falster.[28] According to them, H_2 molecules capture a hole and split into $H^0 + H^+$. In sequence, H^0 will eventually capture a hole and the two H^+ bind to boron via a coulombic interaction.

The mechanism behind Reaction No. 2 was put forward by Pritchard *et al.*[31] and was theoretically investigated by Coutinho *et al.*[54] In this mechanism, H_2 molecules first diffuse to and are captured by boron atoms, forming an intermediate $(BH - H^-)^*$ complex. Two further possible pathways exist. The complex could capture a hole, resulting in a $(BH - H^0)^*$ structure. The neutral hydrogen would then escape, capture another hole, and finally bind to boron. The other possibility entails the relocation of the H^- to form the acceptor BH_2^-. Subsequent capture of two holes results in the donor state BH_2^+, which eventually dissociates into $BH + H^+$.

TABLE II. List of possible rate-limiting steps of the $H_2 \rightarrow BH$ reaction and their corresponding rate proportionalities, as well as a check whether the respective proportionalities match Eq. (8).

Sub-system $H_2 \rightarrow BH$	Rate $\propto$ to[a]	Match
No. 1. $H_2 \rightarrow H^0 + H^0$	$[H_2]$	✗
No. 2. $H_2 + B^- \rightarrow (BH - H^-)^*$	$[H_2][B^-]$	✓
No. 3. $H_2 + h^+ \rightarrow H^+ + H^0$	$[H_2][B^-]$	✓
No. 4. $H_2 + 2h^+ \rightarrow H^+ + H^+$	$[H_2][B^-]^2$	✗
No. 5. $H_2 + B^- + h^+ \rightarrow BH + H^0$	$[H_2][B^-]^2$	✗
No. 6. $H_2 + B^- + 2h^+ \rightarrow BH + H^+$	$[H_2][B^-]^3$	✗

[a]Assuming $p \approx [B^-]$.

The released H^+ binds to an electrically active boron as the BH complex is energetically more favorable.[54]

Regardless of the possible pathways, Reaction No. 2 will ultimately lead to $BH + H^+$, which is also the case of Reaction No. 6. The important difference is that the latter requires both the capture by boron as well as the capture of two holes to limit the reaction rate, resulting in a $\propto[B^-]^3$ dependence. However, the results of Sec. V [compare Eq. (8)] clearly demonstrate a $\propto[B^-]$ dependence, indicating that the capture of holes is not rate limiting the H_2 dissociation mechanism proposed by Pritchard *et al.*[31]

With the experimental data at hand, it is not possible to discern between Reaction Nos. 2 and 3. However, the theoretical work by Coutinho *et al.*[54] indicates that the boron-assisted dissociation of H_2 requires an activation energy of 1.1 eV, while the activation energy for Reaction No. 3 is presumably ~0.5 eV higher.[39] In addition, the activation energy of 1.1 eV agrees well with the value found in this work (see Sec. V B) and the values found by other authors.[32–34] Therefore, Reaction No. 2 seems to be the most likely pathway for the dissociation of H_2 molecules.

It is worth mentioning that resistivity-based methods cannot distinguish between combinations of species that give rise to the same number of charge carriers (holes in case of *p*-type semiconductors). In our case, this comprises the initial state $H_2 + B^-$ and the intermediate states $(BH - H^-)^*$ or BH_2^-. Similarly, such measurement techniques cannot differentiate between the intermediate states $BH_2^+ + B^-$ and $BH + H^+ + B^-$, or 2BH. A direct measurement of the participating complexes would be necessary for such a task.

As we discuss in more detail in Appendix C, simulating all possible pathways according to Reaction No. 2 is beyond the information gathered solely from resistivity measurements. Nevertheless, the important doping dependence $\propto [B^-]$ is also included in Reaction No. 3, which can be more conveniently simulated. Therefore, we choose to employ Reaction No. 3 in our *detailed kinetic model*. In addition, this reaction proves to be capable enough in describing the experimental data.

B. Subsystem $BH \nrightarrow \mathcal{X}$

For the $BH \rightarrow \mathcal{X}$ transition, we investigate possible reaction pathways involving various hydrogen-related complexes, which are listed in Table III alongside their respective expected rate proportionality.

A direct comparison of the rate proportionality to Eqs. (9) and (10) is only possible if the reaction rates are compatible to a *three-state model*. This compatibility can be achieved by expressing $[H^+]$ and $[H^0]$ in terms of the intermediate state concentration, i.e., [BH], as similarly done in Ref. 28. To this end, we assume that the interaction $H^+ + B^- \rightleftharpoons BH$ is very fast compared to the timescale of the annealing experiments.[28] Therefore, H^+ species and BH pairs are approximately in equilibrium, with the proportionality $[H^+] \propto [BH]/[B^-]$ [compare Eq. (2)].

Similarly, neutral hydrogen is always in equilibrium with the other charge states of hydrogen. From the Shockley–Read–Hall model,[55,56] the thermal occupancy ratio follows:

$$\frac{[H^+]}{[H^0]} \approx \frac{p_0}{p_1}, \tag{12}$$

TABLE III. List of possible rate-limiting steps of the reaction BH → $\mathcal{X}$, along with their corresponding rate proportionalities as well as a check whether they match Eq. (9). The tick in parentheses indicates a match to Eq. (10). X denotes an undefined hydrogen sink.

Sub-system BH → $\mathcal{X}$	Rate ∝ to[a]	Match
No. 7. $H^+ + BH \rightarrow H_{2C} + B^- + 2h^+$	$[BH]^2/[B^-]$	✗
No. 8. $H^0 + X \rightarrow HX$	$[BH]/[B^-]^2$	✓
No. 9. $H^+ + X \rightarrow HX + h^+$	$[BH]/[B^-]$	(✓)
No. 10. $BH + X \rightarrow HX + B^- + h^+$	[BH]	✗

[a]Re-written according to Eqs. (2) and (12), with $p \approx [B^-]$ and assuming [X] ≈ constant.

where p_1 is the equilibrium hole density when the Fermi level coincides with the donor level of the (+/0) transition (compare, e.g., Ref. 57). Therefore, $[H^0] \propto [H^+]/p_0 \propto [BH]/[B^-]^2$. Note that due to $[H^+]$ and $[H^0]$ being in equilibrium with [BH], the binding of atomic hydrogen to another sink will also reduce the concentration of BH pairs, thus leading to the experimentally observed decrease.

Among the possibilities listed in Table III, it can be seen that Reaction No. 8 yields a kinetic rate that agrees with Eq. (9), whereas the rate proportionality of Reaction No. 9 is a match to Eq. (10). We also want to highlight Reaction No. 7, as it is the one proposed by Voronkov and Falster.[28] It can be seen that this reaction results in a proportionality with respect to [BH] that is not in line with our experimental observations. In general, the formation of any dimeric hydrogen complex (e.g., H_{2C}) can be ruled out, as this would imply a reaction with second order in [BH], while our experimental observation strongly favors a first-order relation [cf. Eq. (9)].

Bearing that in mind, the possibilities in Table III can be narrowed down to reactions leading to a monohydrogen complex (e.g., HX). Among these reactions, only Nos. 8 and 9 are candidates that could explain the observed rate dependencies. Both reactions will be discussed more in the following, with the potential mechanism behind the BH dissociation being discussed separately in Sec. VI E.

C. A detailed kinetic model

Based on our previous analysis, we develop a *detailed kinetic model*, consisting of the following elementary reactions:

$$H_2 + h^+ \rightleftharpoons H^+ + H^0, \tag{13a}$$

$$H^+ + B^- \rightleftharpoons BH, \tag{13b}$$

$$H^0 + X \rightarrow HX. \tag{13c}$$

As already demonstrated with the *abstract three-state model*, neglecting the reverse reaction $B \leftarrow C$ is a valid approximation, which we, thus, also implement in Eq. (13c). The elementary reactions in Eq. (13) are translated into the following reaction rates:

$$\frac{d[H_2]}{dt} = \beta_{H_2}[H^+][H^0] - \alpha_{H_2}[H_2]p, \tag{14a}$$

$$\frac{d[BH]}{dt} = \beta_{BH}[H^+][B^-] - \alpha_{BH}[BH], \tag{14b}$$

$$\frac{d[HX]}{dt} = \tilde{\beta}_{HX}[H^0][X] \approx \beta_{HX}[H^0], \tag{14c}$$

where β and α are rate constants for the formation and dissociation of the corresponding hydrogen complexes, respectively, and p is the hole concentration. As $[H^0]/[H^+] \approx 10^{-7}$ at 163 °C,[57] the concentration of H^0 can be considered to be way below 1×10^{10} cm^{-3}. Despite not knowing X, it is most likely that $[H^0] \ll [X]$. Therefore, we treat the formation of HX as a pseudo-first-order reaction, resulting in the approximated rate coefficient β_{HX} indicated by Eq. (14c).

We follow the proposition by Hamer *et al.*[58] for modeling the interaction between B^- and H^+, in which the rate coefficient α_{BH} is taken from Zundel and Weber,[59]

$$\alpha_{BH} = \left(2.8 \times 10^{14}\ \mathrm{s}^{-1}\right) \exp\left(\frac{-1.28\ \mathrm{eV}}{k_B T}\right), \tag{15}$$

while β_{BH} is calculated assuming a Coulombic interaction (compare, e.g., Mathiot[60])

$$\beta_{BH} = \frac{q^2 D_{H^+}}{\varepsilon_{Si} k_B T}, \tag{16}$$

with Boltzmann constant k_B, temperature T, elementary charge q, permittivity of silicon ε_{Si}, and diffusivity of positively charged atomic hydrogen D_{H^+} as determined by Gorelkinskii and Nevinnyi.[61]

The reaction rates in Eq. (14) are a system of ordinary differential equations, which we solve using Python. This closed system has fixed total concentrations of boron N_B and total hydrogen $[H]_{tot}$ given by

$$N_B = [B^-] + [BH], \tag{17a}$$

$$[H]_{tot} = 2[H_2] + [BH] + [HX] + [H_{at}], \tag{17b}$$

with $[H]_{at}$ being the sum of all atomic hydrogen species, $[H^+]$, $[H^0]$, and $[H^-]$. The fractions of H^+, H^0, and H^- are calculated in each time step using the Shockley–Sah model (compare Sun *et al.*[57]).

We apply the *detailed kinetic model* to the *boron variation* set, annealed at 163 °C. To do so, the H_2 dissociation rate coefficient α_{H_2} is inferred from the fitted k_{AB} values in Fig. 6. With a linear dependence of k_{AB} on the boron concentration [cf. Eq. (8)], it follows that $\alpha_{H_2} = k_{AB}/[B^-]$. The other two rate constants, β_{H_2} and β_{HX}, are treated as free parameters to best fit the experimental data. Note that, for some samples, $[H_2]_{ini}$ needed to be slightly adjusted (compare Appendix D). The final rate constants are listed in Table IV, and the simulation results are shown in Fig. 4 alongside the experimental data.

It can be seen in Fig. 4 that the experimental data are well described by the simulation of the *detailed kinetic model* (solid red lines) using a single set of rate constants. In addition, Fig. 4 shows a simulation assuming that positively charged hydrogen binds to a

TABLE IV. Rate constants corresponding to the reactions in Eq. (14), determined at 163 °C.

α_{H_2}	β_{H_2}	β_{HX}
2.34×10^{-22} cm^3 s^{-1}	2×10^{-12} cm^3 s^{-1}	12 s^{-1}

sink (Reaction No. 9 in Table III) (dotted red lines). For that simulation, Eq. (14c) is slightly adapted to

$$\frac{d[HX]}{dt} = \beta^*_{HX}[H^+]. \quad (18)$$

The *detailed kinetic model* accounting for Eq. (18) is simulated with the same α_{H_2} and β_{H_2} values as in Table IV, and $\beta^*_{HX} = 6 \times 10^{-5}$ s^{-1}. It can be seen that Eq. (18) fails at describing the two highest doped samples, where the simulated BH dissociation occurs earlier than experimentally observed. This demonstrates that the doping dependence of $1/[B^-]$ is not consistent with our data, which validates the analysis in Sec. V A and the derived proportionality $k_{BC} \propto 1/[B^-]^2$.

We conclude that the reaction $H^0 + X \rightarrow HX$ is well-suited to describe our experimental data and leads to a correct doping dependence. Thus, it is the likeliest reaction behind the dissociation of BH pairs.

D. Temperature dependence

In order to investigate the temperature dependence of the *detailed kinetic model*, we apply our model additionally to the *hydrogen* and *temperature variation* sets by adjusting the rate constants α_{H_2}, β_{H_2}, and β_{HX}. We want to highlight that the same rate constants determined at 163 °C (see Table IV) can be applied to fit data from other samples annealed at comparable temperatures. As a consequence, the *detailed kinetic model* can be used to estimate the initial H_2 concentration in case FT-IR measurements are not available. An example for this is given in Appendix A, where we demonstrate the use of this approach to determine $[H_2]_{ini}$ in the sample annealed at 160 °C by Acker *et al.*[34]

For the analysis of temperature dependence using the *detailed kinetic model*, a comparison between simulation and experimental data is not shown, as the resulting graphs are visually indistinguishable from those in Fig. 5. The obtained rate constants are plotted in Fig. 8 against the reciprocal temperature.

For the rate constant of H_2 dissociation, we find a temperature dependence of

$$\alpha_{H_2} = \left((4 \pm 5) \times 10^{-10}\ \text{cm}^3\ \text{s}^{-1}\right) \times \exp\left(-(1.05 \pm 0.05)\ \text{eV}/(k_B T)\right).$$

The activation energy of α_{H_2} is similar to the value of (1.11 ± 0.05) eV determined herein using the *three-state model* and comparable to 1.15 eV as determined by Voronkov and Falster[32] (dashed line in Fig. 8). It is interesting to note that the activation energy of 1.3 eV determined in Ref. 28 is based on experiments that used significantly differently processed samples[29,31] compared

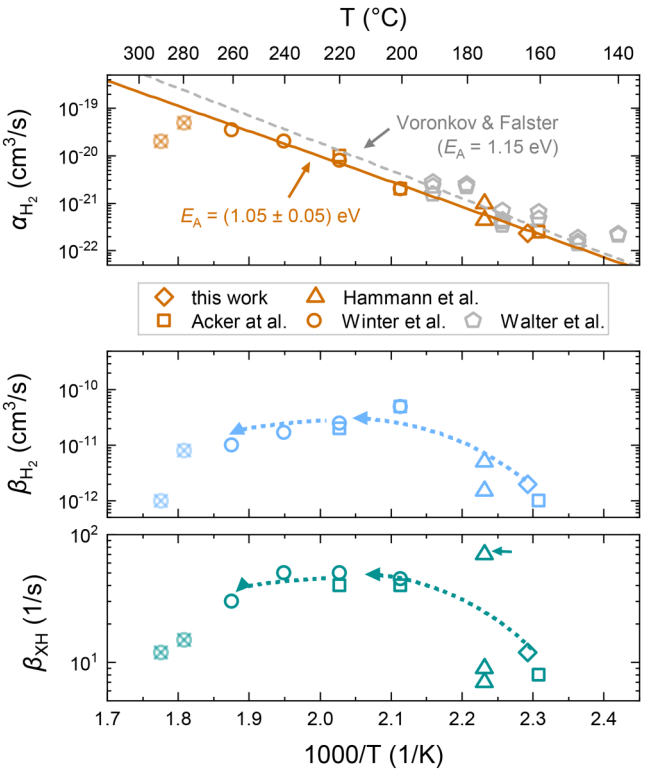

FIG. 8. Temperature dependence of rate constants determined by applying Eq. (14) to the experimental data from different sample sets: *boron* (this work), *hydrogen* (Hammann *et al.*[18,19]), and *temperature variation* (Acker *et al.*[34] and Winter *et al.*[33]). The solid line depicts an Arrhenius law with activation energy of 1.05 eV, while the dashed line shows the temperature dependence as proposed by Voronkov and Falster[32] (the semi-transparent, crossed circle data points are excluded from the fit). The dotted arrows are guides to the eye.

to the ones investigated in the present work. This could indicate that the kinetics of BH reactions is influenced by additional factors arising from differences in sample processing.

Figure 8 also shows the values of α_{H_2} obtained from Walter *et al.*,[62] who used the model from Voronkov and Falster (gray symbols in the top graph). However, these values need to be considered with caution, since they were derived without knowledge on the initial concentrations of H_2 or BH. This might be the primary reason behind the different activation energy of (0.84 ± 0.17) eV determined by Walter *et al.*[62] Moreover, as stated by the authors themselves, their investigation was done without taking the dissociation of BH pairs into account, which also impacts the determination of rate constants. Nevertheless, some data points from Walter *et al.*[62] agree well with the Arrhenius dependence determined by us. It is worth noting that given the uncertainty range reported by Walter *et al.*, there is not necessarily a fundamental disagreement of the results.

In contrast to α_{H_2}, the other two rate coefficients, β_{H_2} and β_{HX}, do not follow a well-defined Arrhenius dependence. Both show first an increase with temperature followed by a slight

decrease above 220 °C (dotted arrows in Fig. 8). The unphysical behavior of these two rate constants is insofar surprising as the temperature dependence of the *abstract three-state model* shows a well-defined Arrhenius-like behavior (compare Fig. 7). Since both β_{H_2} and β_{HX} present a similar trend, it is conceivable that they are related to the same effect. Comparing the individual rates,

$$\frac{d[H_2]}{dt} = \beta_{H_2}[H^+][H^0],$$
$$\frac{d[HX]}{dt} = \beta_{HX}[H^0],$$

one can see that both are linearly dependent on the concentration of neutral hydrogen H^0, which, in turn, is connected to the concentration of H^+. This work uses the Shockley–Sah model as proposed by Sun *et al.*[57] to calculate the fractional concentration of H^0, while $[H^+]$ is related to [BH] through Eq. (14b).

To understand the discrepancy, we analyze how the concentrations of positively charged and neutral atomic hydrogen evolve with temperature. Table V lists the rate constants k_{BA} and k_{BC} determined by the Arrhenius fits of the *abstract three-state model* (compare Fig. 7), along with $[H^+]$ and $[H^0]$ exemplarily calculated for $[BH] = 10^{15}$ cm^{-3} and $N_B = 10^{16}$ cm^{-3} at three chosen temperatures. It can be seen that the concentrations of both H^+ and H^0 increase with increasing temperature.

Focusing first on the subsystem BH ⟞ HX, we can assume that the activation energy of HX formation is the same in both the *abstract three-state model* and in the *detailed kinetic model*, and, therefore, $d(k_{BC}[B])/dT \approx d(\beta_{HX}[H^0])/dT$. However, Table V shows that k_{BC} increases with temperature by three orders between 160 and 240 °C, while $[H^0]$ increases by four orders. A steeper increase of $[H^0]$ compared to k_{BC} implies that β_{HX} has to decrease with temperature to maintain the same reaction rate. A similar argument can be made for the BH ⟞ H_2 transition, where k_{BA} has a slower increase with temperature than the product $[H^+][H^0]$, resulting in a decreasing β_{H_2} value with increasing temperature. Therefore, it is likely that the increase of $[H^0]$ with temperature is not well described by the model of Sun *et al.*,[57] preventing us from determining a physically meaningful temperature dependence for β_{H2} and β_{HX}.

The situation could be different if one simulated the BH ⟞ H_2 subsystem with the boron-enhanced H_2 dissociation pathway (compare Appendix C). However, the non-Arrhenius behavior of β_{HX} is still disadvantageous for a detailed temperature-dependence analysis of the $H^0 + X \rightarrow HX$ reaction as, to the authors' knowledge, no better modeling for H^0 exists today than the one proposed by Sun *et al.*[57]

As a final remark, we draw attention to the two data points from Winter *et al.*[33] at the temperatures of 280 and 290 °C in Fig. 8. For all three rate constants, these points show a downward trend deviating from the expected evolution at lower temperatures. As mentioned before, it is likely that at higher temperatures, further reactions become increasingly important, such as the reverse reaction BH ⟝ HX or the out-diffusion of hydrogen.

TABLE V. Temperature-dependent values of rate constants k_{BA} and k_{BC} from the *three-state model*, compared to $[H^+]$ and $[H^0]$. The latter two are exemplarily calculated by assuming $[BH] = 10^{15}$ cm^{-3} and $N_B = 10^{16}$ cm^{-3}.

	k_{BA} (s^{-1})	k_{BC} (s^{-1})	$[H^+]$ (cm^{-3})	$[H^0]$ (cm^{-3})	$[H^+]$ $[H^0]$ (cm^{-6})
160 °C	5×10^{-8}	4×10^{-8}	2.1×10^{12}	3×10^{5}	6.3×10^{17}
200 °C	8×10^{-6}	1×10^{-6}	1.5×10^{13}	3×10^{7}	4.5×10^{20}
240 °C	6×10^{-4}	2×10^{-5}	8.5×10^{13}	2×10^{9}	1.7×10^{23}

E. On the BH dissociation mechanism

Last, we want to address the implications of our findings to the dissociation mechanism of BH pairs. We propose that, after long-term annealing, neutral hydrogen binds to an unknown sink, termed X. Due to the formation of the energetically favorable HX complex, BH pairs gradually disappear. Although not demonstrated experimentally, our hypothesis seems to be supported by the work from different authors. For instance, Ballutaud *et al.*[38] and Stutzmann *et al.*[63] combined SIMS profiles with effusion experiments to investigate different bonding configurations in hydrogenated silicon. Their results indicate that, upon annealing, hydrogen atoms released from BH pairs in the bulk material do not leave the sample, but rather accumulate in the subsurface region where they form Si–H bonds. Later, Reboredo *et al.*[64] theorized that Si–H clusters, also found in hydrogen-induced platelets, may occur as hydrogen saturated vacancies (VH_4). Curiously, Pritchard *et al.*[31] found an increase in the concentration of VH_4 defects as BH pairs are lost.

These observations are in line with our recent results,[18] where we observed that the onsets of BH pair dissociation and increase in surface-related charge carrier recombination rate are usually synchronized. These results suggest that the loss of BH pairs is connected to a diffusion of hydrogen toward the surface, potentially leading to the formation of surface-near platelets (which would be the cause for the observed increase in surface recombination rate). Importantly, the investigations in our present study support this hypothesis. In that regard, we want to highlight a single β_{HX} rate constant obtained from the data set of Hammann *et al.*[18] This data point is marked by an arrow in the bottom graph of Fig. 8 (at 175 °C), and its value is one order of magnitude larger than the other samples from the same study. This particular sample has a lower thickness of 150 μm compared to all other samples from the various data sets, which have similar thicknesses of around 250 μm. A lower thickness means a shorter path toward the surface and indicates that the dissociation of BH pairs might (at least in part) be limited by a diffusion process toward the surface.

It is, therefore, conceivable that the loss of BH pairs is connected to the movement of hydrogen toward the surface. This could result in the formation of hydrogen platelets and detectable VH_4 complexes. At present, it is unclear whether the diffusion toward the surface is dominated by H^+, which is the dominant atomic state in our *p*-type samples, or by H^0, which has the highest diffusivity of all atomic hydrogen charge states.[39] Moreover, it is conceivable that diffusion toward the surface could be facilitated by an intermediate VH complex,[65] as this complex is known to have a high diffusivity, potentially even higher than that of atomic hydrogen.[65,66] The diffusion mechanism could further be influenced by

the depth-wise hydrogen distribution, facilitating or impeding the diffusion. Further analysis is needed to investigate whether the silicon surface is the final hydrogen sink or whether hydrogen diffuses further into the silicon nitride passivation layer or even diffuses out of the sample.

VII. CONCLUSION

We have investigated the dynamics of BH pairs in crystalline silicon using samples covering a range of $N_B \approx 1.6 \times 10^{15} - 7 \times 10^{16}$ cm^{-3}. Hydrogen was introduced into these samples from hydrogen-rich passivation layers during rapid thermal annealing (RTA). The samples were characterized with FT-IR measurements to determine the initial concentrations of boron–hydrogen pairs $[BH]_{ini}$ and hydrogen molecules $[H_2]_{ini}$. Our results show that, after RTA, only a small percentage of total boron atoms is initially passivated by hydrogen (up to $\sim 2\% \times N_B$). Nevertheless, the measured $[BH]_{ini}$ represents significant shares of the total hydrogen content with increasing doping concentration (up to $\sim 70\% \times [H]_{tot}$).

Upon isothermal dark annealing of the samples at (163 ± 2) °C, changes in hole concentration were quantified via four-point-probe resistivity measurements. These changes were added to $[BH]_{ini}$ determined with FT-IR on a sister wafer to investigate the kinetics of BH pairs. We have tried to describe our experimental data with a model proposed by Voronkov and Falster[28] to no avail. Therefore, we applied an abstract three-state model to perform an in-depth analysis of the kinetics. From this, the doping dependence of the BH-dynamics was derived.

We observe that the dissociation rate of H_2 molecules is directly proportional to the concentration of boron atoms and leads to $-d[H_2]/dt \propto [H_2][B^-]$, which is in accordance with previous findings.[31,54] Upon further annealing, we observe that BH pairs dissociate with hydrogen binding to a new sink and forming an unknown complex termed $\mathcal{X}$. We find that the formation of $\mathcal{X}$ scales inversely with the doping concentration, leading to $d[\mathcal{X}]/dt \propto [BH]/[B^-]^2$. Based on these rate proportionalities, we discuss several pathways to devise possible reaction mechanisms. The dissociation of H_2 molecules occurs most likely via a boron-assisted process, with multiple intermediate steps possibly taking place as theorized by Coutinho *et al.*[54] In particular, we find that the formation of $\mathcal{X}$ can be described well by the reaction of neutral hydrogen binding to an unknown sink X, according to $H^0 + X \rightarrow HX$, in contrast to the hypothesis in which a dimeric complex (H_{2C}) is formed.[28] We extended the available temperature range by adding literature data[33,34] to our analysis. Notably, the activation energy $E_A = (1.11 \pm 0.05)$ eV of the H_2 dissociation rate agrees well with the theoretically calculated value of 1.1 eV.[54]

These results were used as a basis to derive a detailed kinetic model, which accurately describes a large set of experimental data. Using this model, we obtained the corresponding reaction rate constants and investigated their temperature dependence, resulting in a comprehensive, up-to-date picture of BH-dynamics in crystalline silicon. Finally, we discuss the mechanism behind the dissociation of BH pairs, which might be caused by the diffusion of hydrogen toward the surface.

ACKNOWLEDGMENTS

The authors would like to thank Antonio Leimenstoll, Felix Schätzle, Rainer Neubauer, Christian Harmel, Daniel Ourinson, and Andreas Nägele for their help with sample processing. This work was supported by the German Federal Ministry for Economic Affairs and Climate Action (Contract Nos. 03EE1052B and 03EE1052D). The Research Council of Norway is acknowledged for the support of the Norwegian Micro- and Nanofabrication Facility, NorFab (Project No. 295864). Funding for this work was provided by the Norwegian Research Council through the Research Center for Sustainable Solar Cell Technology (FME SUSOLTECH, No. 257639). Pedro Vieira Rodrigues wants to acknowledge the Konrad-Adenauer Stiftung for funding his Master's studies and Benjamin Hammann wants to acknowledge the Stiftung Nagelschneider for funding his dissertation project.

AUTHOR DECLARATIONS

Conflict of Interest

The authors have no conflicts to disclose.

Author Contributions

P. Vieira Rodrigues: Conceptualization (equal); Data curation (equal); Formal analysis (equal); Investigation (lead); Methodology (equal); Software (equal); Visualization (equal); Writing – original draft (lead); Writing – review & editing (equal). **B. Hammann:** Conceptualization (equal); Data curation (equal); Formal analysis (equal); Software (equal); Validation (equal); Visualization (equal); Writing – original draft (equal); Writing – review & editing (lead). **N. Aßmann:** Data curation (equal); Formal analysis (equal); Investigation (equal); Writing – review & editing (equal). **J. Schön:** Formal analysis (equal); Methodology (equal); Validation (equal); Writing – original draft (supporting); Writing – review & editing (equal). **W. Kwapil:** Conceptualization (equal); Project administration (equal); Supervision (equal); Writing – original draft (supporting); Writing – review & editing (equal). **T. Niewelt:** Conceptualization (equal); Supervision (equal); Writing – review & editing (equal). **F. Schindler:** Project administration (equal); Supervision (equal); Writing – review & editing (equal). **E. V. Monakhov:** Project administration (equal); Supervision (equal); Writing – review & editing (equal). **M. C. Schubert:** Project administration (equal); Supervision (equal); Writing – review & editing (equal).

DATA AVAILABILITY

The data that support the findings of this study are available from the corresponding author upon reasonable request.

APPENDIX A: DETERMINATION OF $[BH]_{ini}$ AND $[H_2]_{ini}$ FOR THE TEMPERATURE VARIATION SAMPLE SET

The *temperature variation* sample set consists of data from Acker *et al.*[34] and Winter *et al.*,[33] which cover temperature ranges from 160 to 220 °C and from 200 to 290 °C, respectively. These data were obtained through resistivity measurements, resulting in information solely about $-\Delta p_0$. However, for an accurate

investigation of the BH-dynamics, knowledge on $[BH]_{ini}$ and $[H_2]_{ini}$ is necessary. In the following, we describe our approach for estimating both quantities.

In the studies from Acker *et al.*[34] and Winter *et al.*,[33] most of the samples show a saturated change in hole concentration $-\Delta p_{0,sat}$, which is always lower than the initial value $-\Delta p_{0,ini}$. Such a behavior implies that all BH pairs (including those initially present) are dissociated in the saturated state. Therefore, the initial concentration of BH pairs can be derived from the difference $\Delta p_{0,sat} - \Delta p_{0,ini} \approx [BH]_{ini}$. This estimation approach is also employed in Refs. 33 and 34. We further assume that all samples within a study are prepared similarly and, thus, feature the same initial concentrations of BH and H_2. This allows, for instance, an estimation of $[BH]_{ini}$ in the sample of Acker *et al.*[34] annealed at 160 °C, for which no saturation is visible in the investigated annealing timescale.

After calculating $[BH]_{ini}$, the value of $[H_2]_{ini}$ can be estimated as a free parameter as long as the rate constants are known. In this case, the rate constants can be easily extracted from another study performed at the same temperature. Therefore, our estimation of $[H_2]_{ini}$ is based on the fact that different studies share common annealing temperatures. The process of determining $[H_2]_{ini}$ is represented by a violet arrow in Fig. 9. For this process, we apply the *detailed kinetic model* described in Sec. VI.

We first use the rate constants at 163 °C obtained from the present work to fit the data from Acker *et al.*[34] at 160 °C and find their $[H_2]_{ini}$. The value of $[H_2]_{ini}$ found this way is used as a fixed parameter to iterate the kinetic model and obtain best-fit rate constants. With a known value of $[H_2]_{ini}$ for Acker's data, the rate constants at 200 and 220 °C are obtained (represented by black arrow in Fig. 9). These rate constants are then applied to the data from Winter *et al.*[33] measured at the same annealing temperatures. We find that a single $[H_2]_{ini}$ value describes the temporal evolution at both 200 and 220 °C well. With the obtained $[H_2]_{ini}$ value for Winter's data, the model is iterated and the rate constants for higher temperatures are then determined. The estimated values of $[BH]_{ini}$ and $[H_2]_{ini}$ for the *temperature variation* sample set are listed in Table VI.

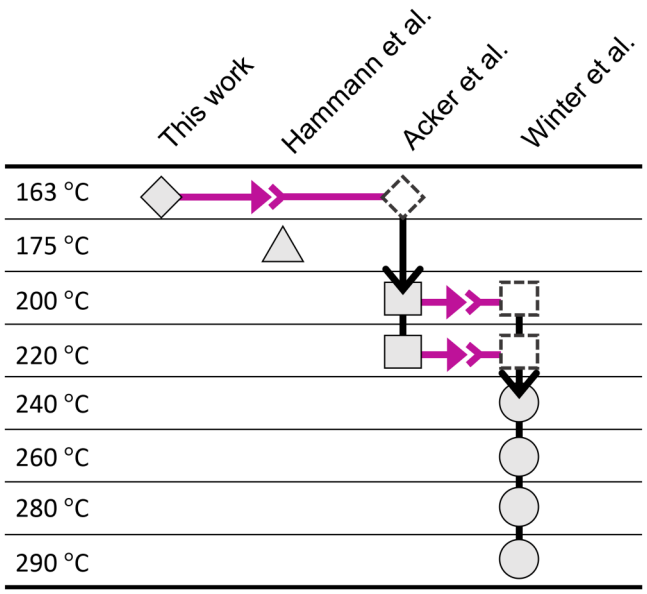

FIG. 9. Schematic depiction of the process of estimating $[H_2]_{ini}$ for the studies by Winter *et al.*[33] and Acker *et al.*[34] Polygons illustrate rate coefficients, which are represented by the same symbols as in Figs. 7 and 8. Violet arrows denote the use of rate constants from a different study at same temperature to estimate $[H_2]_{ini}$. The latter is then used to determine the rate constants at other temperatures of the same study (black arrows).

APPENDIX B: REFERENCE SAMPLE SET

As discussed in Sec. III C 2, our 4PP setup provides high resolution for resistivity measurements. While this leads to a very accurate calculation of $-\Delta p_0$, the results need to be interpreted with caution as the hole concentration can be subject to more than just hydrogen-related effects.

To test the susceptibility of our hydrogen-containing samples to further influence on the hole concentration, we performed 4PP measurements on a *reference sample set*, consisting of bare FZ-Si wafers. These wafers span a doping variation similar to the one used in this work and were not submitted to any hydrogenation process. Therefore, we assume them to be virtually hydrogen-free. More precisely, they underwent only the RCA cleaning, oxidation, and metallization steps (compare also Fig. 1). The comparison between $-\Delta p_0$ measured in the hydrogenated samples (open symbols) and in their hydrogen-free counterparts (black crosses) is shown in Fig. 10 for the two samples of the lowest doping concentration.

It can be seen in Fig. 10 that, in our reference set (black crosses), the lowest doped sample features slight changes in $-\Delta p_0$, while the sample with $N_B = 7.5 \times 10^{15}$ cm^{-3} shows barely any deviations from 0. The other samples with higher doping concentrations also exhibit no detectable variations in hole concentration (data not shown). This fact demonstrates the effectiveness of the oxidation step in removing any potential residual hydrogen found in out-of-the-box FZ-Si wafers[33] and confirms that the samples from our *reference sample set* do not contain significant amounts of hydrogen.

For the lowest doped sample with $N_B = 1.6 \times 10^{15}$ cm^{-3}, we use the small changes in hole concentration observed in the hydrogen-free wafer, $\Delta p_0^{H.free}$ to calculate a corrected $-\Delta p_0^{corr}$ (full symbols in Fig. 10) according to

$$-\Delta p_0^{corr} = -\Delta p_0^{H.cont} + \Delta p_0^{H.free}, \tag{B1}$$

TABLE VI. Initial values for $[BH]_{ini}$ and $[H_2]_{ini}$ determined in this work for the studies by Acker *et al.*[34] and Winter *et al.*[33]

	$[BH]_{ini}$ (cm^{-3})	$[H_2]_{ini}$ (cm^{-3})
Acker *et al.*	5.1×10^{13}	1.6×10^{14}
Winter *et al.*	3.7×10^{13}	3×10^{14}

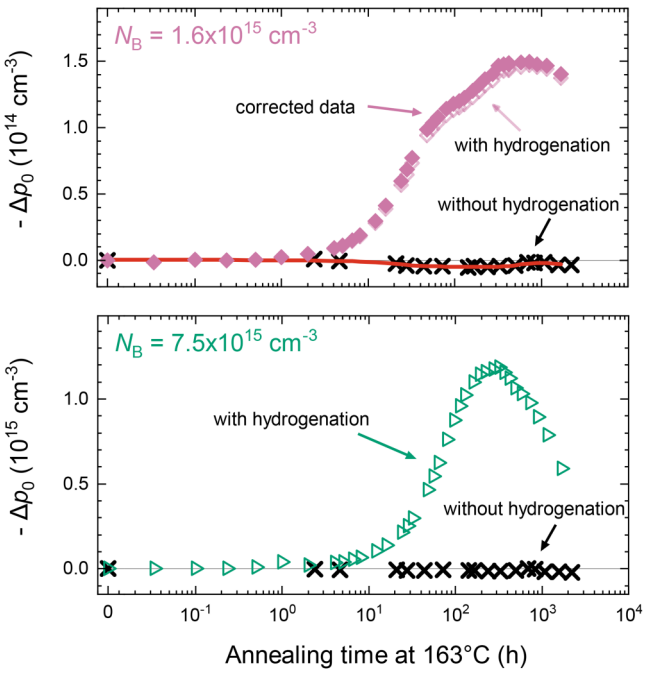

FIG. 10. Comparison between measured changes in hole concentration in our hydrogen-containing samples (open symbols) and in their hydrogen-free counterparts (black crosses), for the two lowest doped samples under dark annealing at (163 ± 2) °C. The red line depicts a lowess filter applied to the hydrogen-free data, whereas full symbols (only in the top graph) represent the hydrogen-containing data after correction. Note the different scales on the *y* axis.

with $-\Delta p_0^{\mathrm{H.cont}}$ representing the change in hole concentration of the sample containing hydrogen. To account for data scattering in the temporal evolution of the hydrogen-free sample, we smooth the values with a *lowess* filter (red line in Fig. 10) and use the result to correct the data of the hydrogen-containing samples (full symbols in Fig. 10).

It is important to note that the hole concentration in the hydrogenated samples might still be influenced by further effects. One influencing factor could be the formation of thermal donors. While one could argue that thermal donor formation should be detectable in the hydrogen-free samples, there are multiple studies reporting that the formation of thermal donors can be enhanced by hydrogen (for example, Refs. 67–69). It is, therefore, possible that some thermal donors might form in the hydrogenated samples, despite the low oxygen concentration of float-zone silicon. Such an effect could explain the non-typical evolution of $-\Delta p_0$ in the lowest doped sample and the slight disagreement between experimental data and simulation in Fig. 4.

APPENDIX C: POTENTIAL REACTION PATHWAYS FOR THE H_2 DISSOCIATION

As described in the main text of this work, we found an activation energy for the $H_2 \rightharpoonup BH$ transition that is very close to the theoretically predicted 1.1 eV for the boron-assisted dissociation of H_2.[31,54] It is, therefore, likely that the dissociation of hydrogen molecules occurs not through the capture of holes but is instead assisted by a boron atom. As the exact reaction pathway is not clear, with potentially many transitional states, it is not possible to extract meaningful information solely based on the experimental data presented in this work. Because of this, our simulation is based on the hypothesized H_2 dissociation through the capture of a hole.[28] In the following, we describe a potential mechanism for the boron-assisted H_2 dissociation process, following the argumentation by Coutinho *et al.*[54]

The first step is the formation of a metastable $(BH - H^-)^*$ configuration,

$$H_2 + B^- \rightleftharpoons (BH - H^-)^*. \tag{C1}$$

Note that the reaction in Eq. (C1) is not detectable with resistivity measurements. In principle, different pathways are possible, each having $(BH - H^-)^*$ as the starting point. For instance, this metastable complex could capture a hole, leading to $(BH - H^0)^*$. The neutral hydrogen could escape, capture another hole, and then react with B^- to form a second BH pair. In this case, we could detect both hole capture processes by means of resistivity measurements, but not distinguish between them.

In an alternative pathway, the negatively charged hydrogen of $(BH - H^-)^*$ relocates to a different site by surmounting an energy barrier of 0.5 eV. This results in the formation of the acceptor BH_2^-,

$$(BH - H^-)^* \rightleftharpoons BH_2^-. \tag{C2}$$

In the next step, two holes are captured to form the donor state BH_2^+,

$$BH_2^- + 2h^+ \rightleftharpoons BH_2^+. \tag{C3}$$

Finally, a H^+ might escape from the BH_2^+ complex,

$$BH_2^+ \rightleftharpoons BH + H^+, \tag{C4}$$

after which H^+ binds to boron to form a second BH pair, which is energetically more favorable than BH_2^+,

$$H^+ + B^- \rightleftharpoons BH. \tag{C5}$$

Along the reaction chain described by Eqs. (C2)–(C5), only Eq. (C3) could be detected with resistivity measurements, since it reduces the hole density.

With multiple transitional states possibly occurring along the overall reaction leading hydrogen molecules to BH pairs, it is not possible to find meaningful values for all respective rate constants from resistivity measurements alone. Assuming that the (simplified) transition $H_2 \rightleftharpoons BH_2^- \rightleftharpoons BH_2^+ \rightleftharpoons 2BH$ takes place, resistivity measurements could only detect the $BH_2^- \rightleftharpoons BH_2^+$ step.

Nevertheless, it is worth mentioning that we find the H_2 dissociation rate to be proportional to the boron concentration

(cf. Fig. 6). This indicates that the rate-limiting process of the path $H_2 \rightleftharpoons BH_2^- \rightleftharpoons BH_2^+ \rightleftharpoons 2BH$ is the $H_2 \rightleftharpoons BH_2^-$ step [see Eq. (C1)], implying that the subsequent (detectable) $BH_2^- \rightleftharpoons BH_2^+$ step probably occurs on a much shorter timescale.

APPENDIX D: COMPARISON OF MEASURED H_2 AND VALUES USED FOR THE SIMULATION

Figure 11 gives an overview on the H_2 concentration measured with low-temperature FT-IR and the values used in different modeling approaches (*three-state fit*, *detailed kinetic model*, and simulating the *VF model*[28,32]). The adjustments for the *three-state fit* and VF model were necessary for some samples as $-\Delta p_{0,\max} > 2[H_2]_{ini}$ was found. In the *detailed kinetic model*, further slight adjustments in H_2 were necessary. This was done for an optimal fit under the condition that all samples at the same temperature are described by a single set of rate constants. Regarding the differences in $[H_2]_{ini}$, we believe that there exist two main reasons. First, since the FT-IR measurements were done months after the resistivity measurements, we do not want to rule out the possibility of an $H_2 \rightarrow BH$ transformation already during the dark storage of these samples. This could explain why $-\Delta p_{0,\max} > 2[H_2]_{ini}$ is observed in the two highest doped samples. On the other hand, the peak temperature during RTA is the significant factor for the final hydrogen concentration, with $[H]_{tot}$ scaling presumably exponentially with the peak temperature. Therefore, at high peak temperatures such as 800 °C, deviations of a few degree centigrade can already lead to strong $[H]_{tot}$ differences.

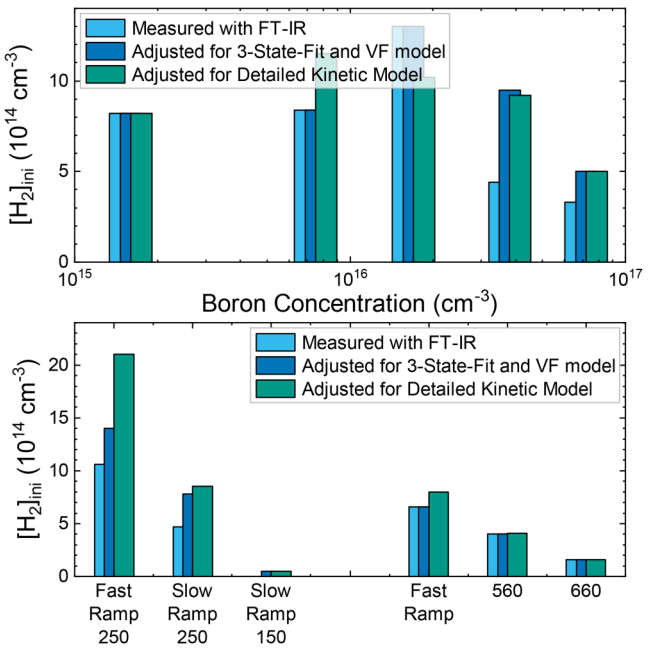

FIG. 11. Comparison between the H_2 concentration measured with FT-IR (light blue) and the values used as input for different modeling approaches: three-state fitting and the model of Voronkov and Falster (dark blue), and detailed kinetic model (green). The comparison is shown for the *boron variation* (top) and *hydrogen variation* (bottom) sample sets. The nomenclature on the *x* axis of the bottom graph is the same as used in Refs. 18 and 19.

REFERENCES

[1]P. Srivastava and U. Singh, "Hydrogen in semiconductors," Bull. Mater. Sci. **19**, 51–60 (1996).
[2]J. I. Pankove and N. M. Johnson, "Introduction to hydrogen in semiconductors," in *Semiconductors and Semimetals* (Elsevier, 1991), Vol. 34, pp. 1–15.
[3]S. J. Pearton, J. W. Corbett, and M. Stavola, *Hydrogen in Crystalline Semiconductors* (Springer Science & Business Media, 2013), Vol. 16.
[4]J. Chevallier and M. Aucouturier, "Hydrogen in crystalline semiconductors," Annu. Rev. Mater. Sci. **18**, 219–256 (1988).
[5]M. Stutzmann and J. Chevallier, *Hydrogen in Semiconductors* (Elsevier, 2012).
[6]M. Stavola, "Hydrogen in semiconductors," AIP Conf. Proc. **671**, 21–32 (2003).
[7]B. J. Hallam, P. G. Hamer, A. M. Ciesla née Wenham, C. E. Chan, B. Vicari Stefani, and S. Wenham, "Development of advanced hydrogenation processes for silicon solar cells via an improved understanding of the behaviour of hydrogen in silicon," Progr. Photovolt.: Res. Appl. **28**, 1217–1238 (2020).
[8]A. Cuevas, M. J. Kerr, and J. Schmidt, "Passivation of crystalline silicon using silicon nitride," in *Proceedings of the 3rd World Conference on Photovoltaic Energy Conversion, 2003* (IEEE, 2003), Vol. 1, pp. 913–918.
[9]J. Schmidt, J. Moschner, J. Henze, S. Dauwe, and R. Hezel, "Recent progress in the surface passivation of silicon solar cells using silicon nitride," in *19th European Photovoltaic Solar Energy Conference: Proceedings of the International Conference* (WIP-Renewable Energies, Munich, 2004), Vol. 1, pp. 391–396.
[10]F. Duerinckx and J. Szlufcik, "Defect passivation of industrial multicrystalline solar cells based on pecvd silicon nitride," Solar Energy Mater. Solar Cells **72**, 231–246 (2002).
[11]R. Preu, E. Lohmüller, S. Lohmüller, P. Saint-Cast, and J. M. Greulich, "Passivated emitter and rear cell—Devices, technology, and modeling," Appl. Phys. Rev. **7**, 041315 (2020).
[12]M. Sheoran, D. S. Kim, A. Rohatgi, H. Dekkers, G. Beaucarne, M. Young, and S. Asher, "Hydrogen diffusion in silicon from plasma-enhanced chemical vapor deposited silicon nitride film at high temperature," Appl. Phys. Lett. **92**, 172107 (2008).
[13]A. G. Aberle, "Overview on sin surface passivation of crystalline silicon solar cells," Solar Energy Mater. Solar Cells **65**, 239–248 (2001).
[14]T. Niewelt, F. Schindler, W. Kwapil, R. Eberle, J. Schön, and M. C. Schubert, "Understanding the light-induced degradation at elevated temperatures: Similarities between multicrystalline and floatzone p-type silicon," Progr. Photovolt.: Res. Appl. **26**, 533–542 (2017).
[15]D. Chen, M. Vaqueiro Contreras, A. Ciesla, P. Hamer, B. Hallam, M. Abbott, and C. Chan, "Progress in the understanding of light-and elevated temperature-induced degradation in silicon solar cells: A review," Progr. Photovolt.: Res. Appl. **29**, 1180–1201 (2021).
[16]M. A. Jensen, A. Zuschlag, S. Wieghold, D. Skorka, A. E. Morishige, G. Hahn, and T. Buonassisi, "Evaluating root cause: The distinct roles of hydrogen and firing in activating light-and elevated temperature-induced degradation," J. Appl. Phys. **124**, 085701 (2018).
[17]J. Schmidt, D. Bredemeier, and D. C. Walter, "On the defect physics behind light and elevated temperature-induced degradation (LeTID) of multicrystalline silicon solar cells," IEEE J. Photovolt. **9**, 1497–1503 (2019).
[18]B. Hammann, N. Assmann, P. M. Weiser, W. Kwapil, T. Niewelt, F. Schindler, R. Søndenå, E. V. Monakhov, and M. C. Schubert, "The impact of different hydrogen configurations on light-and elevated-temperature-induced degradation," IEEE J. Photovolt. **13**, 224–235 (2023).
[19]B. Hammann, N. Aßmann, J. Schön, W. Kwapil, F. Schindler, S. Roder, E. V. Monakhov, and M. C. Schubert, "Understanding the impact of the cooling ramp of the fast-firing process on light- and elevated-temperature-induced degradation," Solar Energy Mater. Solar Cells **259**, 112462 (2023).

[20]R. Zerfaß, J. Simon, A. Herguth, and G. Hahn, "Impact of hydrogen in Ga-doped silicon on maximum LeTID defect density," Sol. RRL **7**(22), 2300501 (2023).
[21]D. Sperber, A. Graf, D. Skorka, A. Herguth, and G. Hahn, "Degradation of surface passivation on crystalline silicon and its impact on light-induced degradation experiments," IEEE J. Photovolt. **7**, 1627–1634 (2017).
[22]K. Kim, R. Chen, D. Chen, P. Hamer, A. Ciesla nee Wenham, S. Wenham, and Z. Hameiri, "Degradation of surface passivation and bulk in p-type monocrystalline silicon wafers at elevated temperature," IEEE J. Photovolt. **9**, 97–105 (2019).
[23]B. Hammann, J. Engelhardt, D. Sperber, A. Herguth, and G. Hahn, "Influencing light and elevated temperature induced degradation and surface-related degradation kinetics in float-zone silicon by varying the initial sample state," IEEE J. Photovolt. **10**, 85–93 (2019).
[24]C. Winter and A. Herguth, "Contacted resistance measurements for the quantification of boron-hydrogen pairs in crystalline silicon," AIP Conf. Proc. **2487**, 130016 (2022).
[25]B. Hammann, L. Rachdi, W. Kwapil, F. Schindler, and M. C. Schubert, "Insights into the hydrogen-related mechanism behind defect formation during light-and elevated-temperature-induced degradation," Phys. Status Solidi (RRL) **15**, 2000584 (2021).
[26]F. Kersten, F. Fertig, K. Petter, B. Klöter, E. Herzog, M. B. Strobel, J. Heitmann, and J. W. Müller, "System performance loss due to LeTID," Energy Procedia **124**, 540–546 (2017).
[27]D. C. Walter, D. Bredemeier, R. Falster, V. V. Voronkov, and J. Schmidt, "Easy-to-apply methodology to measure the hydrogen concentration in boron-doped crystalline silicon," Solar Energy Mater. Solar Cells **200**, 109970 (2019).
[28]V. V. Voronkov and R. Falster, "Formation, dissociation, and diffusion of various hydrogen dimers in silicon," Phys. Status Solidi B **254**, 1600779 (2017).
[29]M. Binns, R. Newman, S. McQuaid, and E. C. Lightowlers, "Hydrogen solubility and defects in silicon," in *Materials Science Forum* (Trans Tech Publications, 1994), Vol. 143, pp. 861–866.
[30]S. McQuaid, M. Binns, R. Newman, E. Lightowlers, and J. Clegg, "Solubility of hydrogen in silicon at 1300 °C," Appl. Phys. Lett. **62**, 1612–1614 (1993).
[31]R. Pritchard, J. Tucker, R. Newman, and E. Lightowlers, "Hydrogen molecules in boron-doped crystalline silicon," Semicond. Sci. Technol. **14**, 77 (1999).
[32]V. V. Voronkov and R. Falster, "Generation and loss of hydrogen-boron pairs in fired silicon wafers," Mater. Sci. Semicond. Process. **167**, 107796 (2023).
[33]C. Winter, J. Simon, and A. Herguth, "Study on boron–hydrogen pairs in bare and passivated float-zone silicon wafers," Phys. Status Solidi A **218**, 2100220 (2021).
[34]Y. Acker, J. Simon, and A. Herguth, "Formation dynamics of BH and GaH-pairs in crystalline silicon during dark annealing," Phys. Status Solidi A **219**, 2200142 (2022).
[35]S. McQuaid, R. Newman, J. Tucker, E. Lightowlers, R. Kubiak, and M. Goulding, "Concentration of atomic hydrogen diffused into silicon in the temperature range 900–1300 °C," Appl. Phys. Lett. **58**, 2933–2935 (1991).
[36]S. McQuaid, R. Newman, and E. C. Lightowlers, "Measurements relating to the solubility of hydrogen in silicon at high temperatures," in *Materials Science Forum* (Trans Tech Publications, 1992), Vol. 83, pp. 93–98.
[37]M. Stutzmann, W. Beyer, L. Tapfer, and C. Herrero, "States of hydrogen in crystalline silicon," Physica B **170**, 240–244 (1991).
[38]D. Ballutaud, P. De Mierry, J. Pesant, R. Rizk, A. Boutry-Forveille, and M. Aucouturier, "Hydrogen effusion from monocrystalline B-doped silicon," in *Materials Science Forum* (Trans Tech Publications, 1992), Vol. 83, pp. 45–50.
[39]D. Gomes, V. P. Markevich, A. R. Peaker, and J. Coutinho, "Dynamics of hydrogen in silicon at finite temperatures from first principles," Phys. Status Solidi B **259**, 2100670 (2022).
[40]C. Herring, N. Johnson, and C. G. Van de Walle, "Energy levels of isolated interstitial hydrogen in silicon," Phys. Rev. B **64**, 125209 (2001).
[41]A. Herguth and C. Winter, "Methodology and error analysis of direct resistance measurements used for the quantification of boron–hydrogen pairs in crystalline silicon," IEEE J. Photovolt. **11**, 1059–1068 (2021).
[42]N. E. Grant, V. P. Markevich, J. Mullins, A. R. Peaker, F. Rougieux, and D. Macdonald, "Thermal activation and deactivation of grown-in defects limiting the lifetime of float-zone silicon," Phys. Status Solidi (RRL) **10**, 443–447 (2016).
[43]O. John, J. Paschen, A. De Rose, B. Steinhauser, G. Emanuel, A. A. Brand, and J. Nekarda, "Laser metal bonding (LMB)-low impact joining of thin aluminum foil to silicon and silicon nitride surfaces," Proc. CIRP **94**, 863–868 (2020).
[44]P. M. Weiser, E. Monakhov, H. Haug, M. S. Wiig, and R. Søndenå, "Hydrogen-related defects measured by infrared spectroscopy in multicrystalline silicon wafers throughout an illuminated annealing process," J. Appl. Phys. **127**, 065703 (2020).
[45]C. Sah, J. Y. Sun, and J. J. Tzou, "Deactivation of the boron acceptor in silicon by hydrogen," Appl. Phys. Lett. **43**, 204–206 (1983).
[46]J. I. Pankove, R. O. Wance, and J. E. Berkeyheiser, "Neutralization of acceptors in silicon by atomic hydrogen," Appl. Phys. Lett. **45**, 1100–1102 (1984).
[47]R. Pritchard, M. Ashwin, J. Tucker, R. Newman, E. Lightowlers, M. Binns, S. McQuaid, and R. Falster, "Interactions of hydrogen molecules with bond-centered interstitial oxygen and another defect center in silicon," Phys. Rev. B **56**, 13118 (1997).
[48]A. Fell, J. Schön, M. C. Schubert, and S. W. Glunz, "The concept of skins for silicon solar cell modeling," Solar Energy Mater. Solar Cells **173**, 128–133 (2017).
[49]A. Fell, see https://www.quokka3.com/ for information about "Quokka 3" (last accessed December 10, 2022).
[50]D. Klaassen, "A unified mobility model for device simulation—I. Model equations and concentration dependence," Solid-State Electron. **35**, 953–959 (1992).
[51]D. Klaassen, "A unified mobility model for device simulation—II. Temperature dependence of carrier mobility and lifetime," Solid-State Electron. **35**, 961–967 (1992).
[52]M. Newville, R. Otten, A. Nelson, A. Ingargiola, T. Stensitzki, D. Allan, A. Fox, F. Carter, Michał, R. Osborn, D. Pustakhod, Lneuhaus, S. Weigand, Glenn, C. Deil, Mark, A. L. R. Hansen, G. Pasquevich, L. Foks, N. Zobrist, O. Frost, A. Beelen, Stuermer, Azelcer, A. Hannum, A. Polloreno, J. H. Nielsen, S. Caldwell, A. Almarza, and A. Persaud, "lmfit/lmfit-py: 1.0.3" (2021).
[53]B. Hammann, "The influence of hydrogen on silicon solar cells: Investigating the link to degradation mechanisms," Dissertation (Universität Freiburg, Freiburg, 2023).
[54]J. Coutinho, D. Gomes, V. J. B. Torres, T. O. Abdul Fattah, V. P. Markevich, and A. R. Peaker, "Theory of reactions between hydrogen and group-III acceptors in silicon," Phys. Rev. B **108**, 014111 (2023).
[55]W. Shockley and W. T. Read, "Statistics of the recombinations of holes and electrons," Phys. Rev. **87**, 835–842 (1952).
[56]R. N. Hall, "Electron-hole recombination in germanium," Phys. Rev. **87**(2), 387 (1952).
[57]C. Sun, F. E. Rougieux, and D. Macdonald, "A unified approach to modelling the charge state of monoatomic hydrogen and other defects in crystalline silicon," J. Appl. Phys. **117**, 045702 (2015).
[58]P. Hamer, B. Hallam, R. Bonilla, P. Altermatt, P. Wilshaw, and S. Wenham, "Modelling of hydrogen transport in silicon solar cell structures under equilibrium conditions," J. Appl. Phys. **123**, 043108 (2018).
[59]T. Zundel and J. Weber, "Trap-limited hydrogen diffusion in boron-doped silicon," Phys. Rev. B **46**, 2071 (1992).
[60]D. Mathiot, "Modeling of hydrogen diffusion in n-and p-type silicon," Phys. Rev. B **40**, 5867 (1989).
[61]Y. V. Gorelkinskii and N. Nevinnyi, "EPR of interstitial hydrogen in silicon: Uniaxial stress experiments," in *C, H, N and O in Si and Characterization and Simulation of Materials and Processes* (Elsevier, 1996), pp. 133–137.

[62]D. C. Walter, V. V. Voronkov, R. Falster, D. Bredemeier, and J. Schmidt, "On the kinetics of the exchange of hydrogen between hydrogen–boron pairs and hydrogen dimers in crystalline silicon," J. Appl. Phys. **131**, 165702 (2022).
[63]M. Stutzmann and M. S. Brandt, "Deuterium effusion measurements in doped crystalline silicon," J. Appl. Phys. **68**, 1406–1409 (1990).
[64]F. Reboredo, M. Ferconi, and S. Pantelides, "Theory of the nucleation, growth, and structure of hydrogen-induced extended defects in silicon," Phys. Rev. Lett. **82**, 4870 (1999).
[65]M. A. Roberson and S. K. Estreicher, "Vacancy and vacancy-hydrogen complexes in silicon," Phys. Rev. B **49**, 17040–17049 (1994).
[66]B. L. Sopori, K. Jones, and X. J. Deng, "Observation of enhanced hydrogen diffusion in solar cell silicon," Appl. Phys. Lett. **61**, 2560–2562 (1992).
[67]A. Brown, M. Claybourn, R. Murray, P. Nandhra, R. Newman, and J. Tucker, "Enhanced thermal donor formation in silicon exposed to a hydrogen plasma," Semicond. Sci. Technol. **3**, 591 (1988).
[68]R. Newman, J. Tucker, A. Brown, and S. McQuaid, "Hydrogen diffusion and the catalysis of enhanced oxygen diffusion in silicon at temperatures below 500 °C," J. Appl. Phys. **70**, 3061–3070 (1991).
[69]H. Stein and S. Hahn, "Hydrogen introduction and hydrogen-enhanced thermal donor formation in silicon," J. Appl. Phys. **75**, 3477–3484 (1994).